Fabrication and energetic characterization of micro and nano sized Al/CuO core-shell particles

by

Yiqi Zhang

A thesis

presented to the University of Waterloo

in fulfilment of the

thesis requirement for the degree of

Master of Applied Science

in

Mechanical and Mechatronics Eng (Nanotechnology)

Waterloo, Ontario, Canada, 2019

Examining Committee Membership

The following served on the Examining Committee for this thesis. The decision of the Examining Committee is by majority vote.

Supervisors

NAME	John Z. Wen
Title	Associate professor
NAME	Yuning Li
Title	Professor

Internal Member

NAME	Jean-Pierre Hickey
Title	Assistant Professor

Internal Member

NAME	Adrian Gerlich
Title	Associate Professor

Author's Declaration

I hereby declare that I am the sole author of this thesis. This is a true copy of the thesis, including any required final revisions, as accepted by my examiners.

I understand that my thesis may be made electronically available to the public.

Abstract

Al/CuO is a well-studied thermite system enabling high energy release and production of pure copper from the reaction. Common Al/CuO thermites include composites of Al and CuO micro- and nano-particles, multi-layered Al and CuO structures, and agglomeration of particles. There is a gap in fabrication and characterization of individual and spherical Al/CuO core-shell particles that have promising application in mobile delivery of energy.

A new synthesis method for producing spherical Al/CuO particles with a core-shell structure is introduced in this thesis. The compositions and microstructures of as-produced samples are investigated during fabrication and over the thermite reaction through which the core-shell geometry is characterized and the reaction mechanism is studied.

Spherical Al particles with two distinct diameters – 40 nm and 1 μm – are coated with CuO shell. Their thermochemical properties are measured in with Thermogravimetric analysis and Differential Scanning Calorimeter. With the help of XRD, XPS, TEM and SEM/EDS, the microstructures and the compositions are investigated. The combustion properties of these two samples are studied using laser ignition and a high-speed camera.

It is concluded that the developed synthesis method is able to produce the core-shell samples with satisfying ignition parameters and energy release. The reaction mechanism and combustion properties of those representative core-shell particles with different sizes are different, where the micro-sized sample could be dominant by condensed phase reaction and nano-sized sample could be dominant by heterogeneous reaction.

Acknowledgement

First and foremost, I would like to thank my supervisors Prof. John Z. Wen and Prof. Yuning Li for giving me the opportunity to perform this very interesting study, for all the guidance and patience they gave me. They always encourage me to explore all the possibilities behind the experiments and they taught me step by step how to do research with great patience.

I would like thank to my committee members, Professor Jean-Pierre Hickey and Professor Adrian Gerlich for their valuable time and constructive suggestions on my thesis

I feel grateful to have the opportunity to work with all the researchers and I want to thank all the members of Laboratory for Emerging Energy Research (LEER) for their valuable help. I had the honor to work with Dr. Hongtao Sui, Dr. Pei Zhao, Boyu Li, Lauren LeSergent and Jenner Ngai and they really gave me a lot of help and suggestion on my study. Especially thanks Florin Saceleanu who helped me conduct the laser ignition tests. It was a great pleasure to work with you all.

Special thanks to my parents, my family, my boyfriend and my friends for their love and support. Their encouragement helps me a lot during tough time. They are considered dominant by condensed phase reaction and heterogeneous reaction respectively through the analysis of results so far.

Table of Contents

Examining Committee Membership ..... **ii**

Author's Declaration ..... **iii**

Acknowledgement ..... **v**

List of figures ..... **viii**

List of tables ..... **xi**

1.0 Introduction **1**

1.1Motivation and Problem statement 1

1.2 Research Objects 2

1.3 Thesis Organization 2

2.0 Literature Review **4**

2.1 Introduction to energetic materials 4

2.2 Types of thermites 6

2.3 Applications of thermites 10

2.4 Fabrication methods of thermite composites 13

2.5 Review of thermite reaction of Al with CuO 21

2.6 Characterization methods 24

2.6.1 Thermogravimetric Analysis (TGA)/Differential Scanning Calorimetry 24

2.6.2 X-Ray Diffraction (XRD) 25

2.6.3 Scanning Electron Microscopy /Energy Dispersive X-ray Spectrometer 26

2.6.4 X-ray Photoelectron Spectroscopy (XPS) 27

2.6.5 Transmission electron microscopy (TEM) 28

2.6.6 High speed camera and Photodiode 28

3.0 Experimental 29

3.1 Synthesis methods 29

3.2 Determination of the composition and structure of the Al/CuO microparticles 31

3.3 Determination of the composition and structures of Al/CuO nanoparticles 36

4.0 Results and discussion 41

4.1 Thermochemical properties of samples under low heating rates 41

4.1.1 DSC and TGA results of Al/CuO microparticles 41

4.1.2 DSC and TGA results of Al/CuO nanoparticles 45

4.2 Effects of equivalence ratio on laser ignition of core-shell Al/CuO particles 48

4.2.1 Introduction 48

4.2.2 Experimental 50

4.2.3 Results and discussion 52

4.2.4 Summary 55

4.3Determination of reaction mechanism of Al/CuO core-shell structures 56

4.3.1 Introduction 56

4.3.2 Discussion on the reaction mechanism of the Al/CuO micro-particles 58

5.3.3 Study of reaction mechanism of Al/CuO nano-sized particles 60

5.0 Summary and future work 62

5.1 Summary 62

5.2 Contributions 64

5.3 Future work 65

References 66

List of figures

Figure2. 1 Reaction enthalpy of monomolecular energetic materials and metal fuels[5] 4

Figure2. 2 Comparison of different structures of thermites. 6

Figure2. 3 DSC traces for different thermites prepared with mixing of Al and oxidizer nanopowder[14] 7

Figure2. 4 (a) 3D view of the structure of the micro-actuator. (b) Schematic of the working principle for micro-actuator from Gustavo et al.[19] 11

Figure2. 5 Schematic of reactor for melting of municipal solid waste incinerator fly ash by waste-derived thermite reaction[25] 12

Figure2. 6 The working principle of alarm switch operated remotely using a focused-laser-assisted igniter from Nam-su et al.[26] 13

Figure2. 7 SEM image of Al/CuO synthesize by arrested reactive milling with different milling durations and different morphology of the samples by Swati et al.[27] 14

Figure2. 8 Process of self-assembly synthesis of Al/Fe_2O_3 thermite, from JL Cheng[42] 16

Figure2. 9 Schematics of the fabrication process of the CuO/Al core/shell NWs and the corresponding SEM images by Ohkura et al .[44] 17

Figure2. 10 SEM image of the cross-section view of layered Al/Fe_2O_3 composite by Hongtao et. Al[29] 18

Figure2. 11 SEM cross-section images of multilayers magnetron sputtered. A: 3 layers CuO(1 μm)/Al(1 μm)/CuO(1 μm). B: 10 layers of CuO(100 nm)/Al(100 nm).[33] 20

Figure2. 12 A schematic of the shock tube experiments. Left: Prior to arrival of the incident shock at the endwall. Right: After shock reflection.[53] 23

Figure2. 13 the NETZSCH STA 449 F3 Jupiter DSC machine used for this thesis..... 25

Figure2. 14 INEL Powder X-ray Diffractometer..... 26

Figure3. 1 Schematic of synthesis procedure of Al/CuO micro-particles with a core-shell structure……..30

Figure3. 2 Experimental procedures of synthesis of the samples..... 30

Figure3. 3 XRD spectra of the sample during fabrication: (a) before and (b) after annealing. The sample after reactions with the DSC test: (c)..... 32

Figure3. 4 XPS spectra of the sample: (a) feature peaks of Al, (b) feature peaks of Cu..... 32

Figure3. 5 TEM images of (a) as-fabricated Al/CuO core-shell micro-particle; (b) enlarged edge of the as-fabricated micro-particle; and (c) as-purchased Al micro-particle with a passivation layer..... 33

Figure3. 6 (a) TEM image of the sample, (b) EDS mapping result of the particle, (c) EDS mapping result of Al and (d) EDS mapping of Cu..... 34

Figure3. 7 (a) SEM image of as-fabricated Al/CuO sample; (b) and (c): EDAX elemental mapping of Al and Cu, respectively..... 36

Figure3. 8 XRD results of sample1 with equivalence ratio of 1: (a) sample after annealing, (b) sample heated up 800℃° in Argon and (c) sample heated up to 1200℃° in Argon..... 37

Figure3. 9 SEM image of Al/CuO nano-sized sample with equivalence ratio of 1..... 38

Figure3. 10 TEM images of: (a) as-purchased Al nanoparticles with average diameter of 40 nm; (b) assembled Al/CuO sample 39

Figure3. 11 EDS of the assembled Al/CuO sample at the same location of the SEM image..... 40

Figure4. 1 DSC and TGA (mass) results of the three samples with different equivalence ratios: (1) 5, (2) 3 and (3) 1, respectively……41

Figure4. 2 DSC traces for reactions of CuO/Al core-shell particles with heating rates of 10 K/min(1), 20K/min(2) and 30K/min(3) (b) Analysis of DSC traces 45
Figure4. 3 DSC results of sample1, sample2, and sample3 with equivalence ratios of 1, 2 and 3 respectively 47
Figure4. 4 TGA results of sample1, sample2, and sample3 with equivalence ratios of 1, 2 and 3 respectively 48
Figure4. 5 Schematic of laser ignition setup..... 50
Figure4. 6 Determination of the ignition delay of the thermite reaction from photodiode signals for sample 4..... 51
Figure4. 7 Determination of burning rate 52
Figure4. 8 Ignition delay of samples with different equivalent ratio..... 53
Figure4. 9 Comparison of flame expansion at the same time scale between micro-sample and nano-sample 54
Figure4. 10 The flame propagation feature of nano-sample with equivalence ratio of 1 54
Figure4. 11 Reaction mechanisms proposed for Al/CuO system 57
Figure4. 12 SEM image and EDS mapping of the Al/CuO particle after the reaction..... 60
Figure4. 13 Comparison of flame of (a) sample with ER=1, (b) sample with ER=3 61

List of tables

Table2. 1 properties of selected thermites, modified from Fischer et al.[15] 8

Table2. 2 comparison of preparation methods discussed in this chapter of the structure formed, cost, scalability, impurity level and safety 21

Table 4- 1 The thermochemical properties of samples with core-shell structure 42

Table 4- 2 Sample properties and the derived activation energy data for the core-shell micro-particles in this study, the reference sample and the literature Al oxidation in oxygen..... 43

Table 4- 3 The thermal characteristics of sample1, 2 and 3 of Al/CuO nanoparticles..... 46

Table4- 4 The ignition delay of samples with different equivalence ratios 53

1.0 Introduction

1.1Motivation and Problem statement

Metal-based energetic materials, also known as thermites composites, have shown a promising application in metal refining, welding, pyrotechnics and munitions since their higher energy density is compared to other energetic materials.[1,2] Thermites composed of fuel (metal) and oxidiser (metal oxide) which release stored chemical energy upon external stimulation, such as heat or current. Aluminium is the most commonly used fuel material due to its abundance on the earth and high oxidation energy release, and magnesium, zinc and titanium are also investigated as a fuel source.[3,4] For the oxidiser, many different types of materials could be utilised including CuO, Fe_2O_3, MoO_3 and NiO.

Nowadays, more applications for thermites in Microelectromechanical systems (MEMS) require more precise control of the characteristics of the thermites, including heat release, gas generation and initiation temperature. The main product of this thesis, core-shell spherical particles, in contrast to other structures, such as films and arrays, are attractive in applications involving mobile particles. Meanwhile, the low cost of raw materials would assist in promoting large-scale production for application in more areas.

The performance of microparticle and nano-particle composites depends heavily on mixing and packing, and different thermites with unique features could be applied in some certain areas like molecular delivery systems. Thus, it is vital to explore how structures, sizes and composition affects the characteristic of this thermite and to develop more advanced thermites based on these conclusions. Additionally, the investigation of the reaction mechanism for both microparticles and nano-particles composites would support the future modification on this type of thermites.

1.2 Research Objects

The successful synthesis of Al/CuO thermites with spherical core-shell structures is the first goal of this thesis, since most updated core-shell structures are based on wires and sputtering. Both micro- and nano-scale Al particles would be utilized as the raw material, since they could target different requirements. Microscale products whose thermal characteristics are comparable with some nano-thermites could be used for the large-quantity requirement with advanced properties and low cost at the same time, while nano-scale products are more suitable for even smaller devices with an extremely high-performance requirement. Importance should be placed on how different structures, equivalence ratio and sizes would influence the thermal performance of the thermites. The performance of thermites under laser ignition has also been measured to explore the difference of the thermites under high heating rates. The reaction mechanism for both micro-thermites and nano-thermites of Al/CuO would be discussed based on the thermal performance under different heating rates, and some literature modelling results would be utilised to compare the experimental data.

1.3 Thesis Organization

Chapter 2 provides a literature review of relevant thermites, and their different synthesis methods, characterization methods, and an introduction of proposed applications for thermites. In chapter 3, the fabrication method for producing spherical Al/CuO core-shell particles is introduced first, then a detailed description of the compositions and microstructures of samples will be given. In chapter 4, the experimental results and corresponding discussion will be outlined, in which the thermochemical properties of two distinct samples will be discussed through DSC measurement and laser ignition results. Then the reaction mechanisms for these two samples will be studied

based on previous experiments in chapter 4. A summary of all the results and contributions of this thesis will be shown in chapter 5, along with the future work discussion.

2.0 Literature Review

2.1 Introduction to energetic materials

There are many types of energetic materials that could store much energy, since they have been developed for hundreds of years. TNT, RDX and CL-20 are common species of the monomolecular compound of energetic materials, which are famous for fast reaction rates,[5] while the relatively low energy densities of this type material make metal-based energetic material suitable for application with requirement of high energy release. The comparison of energy densities for different types of energetic materials is shown in Figure 2.1.[5]

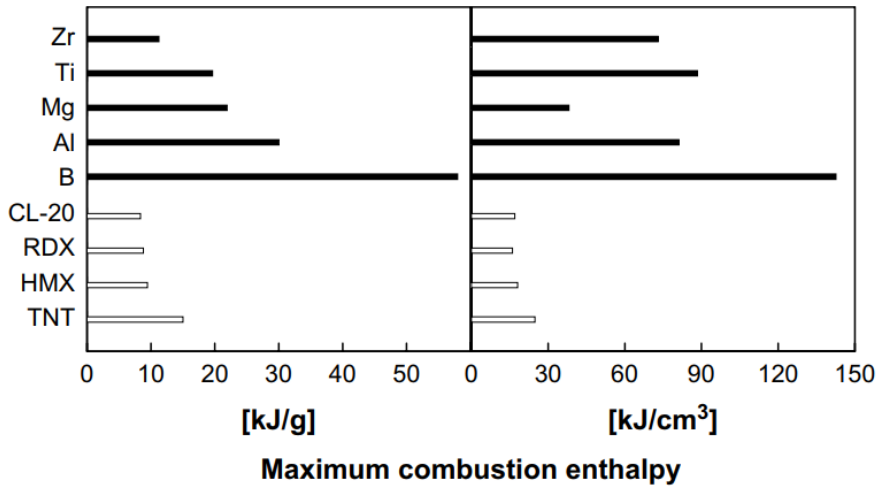

Figure2. 1 Reaction enthalpy of monomolecular energetic materials and metal fuels[5]

In 1908, Goldschmidt first defined the word "thermit" as the exothermic oxidation-reduction reaction between aluminium and a metallic oxide, which could generate a large amount of heat rapidly.[6] Later, the concept of thermite reaction was broadened to the oxidation-reduction reaction of a metal and metallic or non-metallic oxide. The oxygen from the oxide will form more

stable bonds with the metal during the reaction, and the reaction is shown below. In this equation, M and AO are the metal (fuel) and the oxide, where MO and A represent the newly formed oxide and metal/non-metal respectively, and ΔH is the heat generated by this reaction.

$$M + AO \rightarrow MO + A + \Delta H \quad \text{(Eq. 2-1)}$$

One important application of traditional termites is to weld metal components by melting the joining one.[7] Moreover, the thermite material used for this application is usually mixed with microscale powder to lower the cost. Due to the longer diffusion distance of mass and heat, a micro-sized powder mixture would have lower reaction rates and longer ignition delay compared to those of monomolecular energetic compounds.[8] The slower reaction rate results in a heat loss, which could cause a quenching effect sometimes. Moreover, micro-sized powder thermites are not very sensitive to triggers, such as impact, friction and electrostatic discharge, creating stricter ignition conditions.[9] For example, to join the railways, pre-heating sources are required to ignite the thermite reaction and heating sources are also required during the process to maintain the thermite reaction due to the huge heat loss, while the research on the relationship between size and thermal properties concluded that smaller scale of thermites with a higher surface to volume ratio could lead to lower activation energy and a lower reaction speed.[10] Researchers developed some new structures introducing nano-particles to meet new requirements for thermites, and the diffusion distance for both mass and heat would be shortened consequently. The homogeneous mixtures of nano-particles significantly improved the performance of thermite reactions. For example, Aumann used 20-50nm Al/MoO_3 nano-thermites to obtain a reaction 1,000 times faster than the conventional thermites.[11] Since the performance of nano-thermites is similar to

monomolecular energetic material, they are also called metastable intermolecular composites (MIC).

The development of a core-shell structure further increased the performance of thermites due to the even larger contact area and shorter diffusion distance for mass. Silicon is the commonly used substrate material and the oxide would grow on the substrate. The metal would be deposited on top of oxide through magnetron sputtering or vapour deposition.[12,13] As illustrated by Figure 2.2, the contact areas for all three core-shell structures between metal and oxide are significantly increased when compared to power mixtures and, thus, the thermite reaction would have a lower onset temperature.

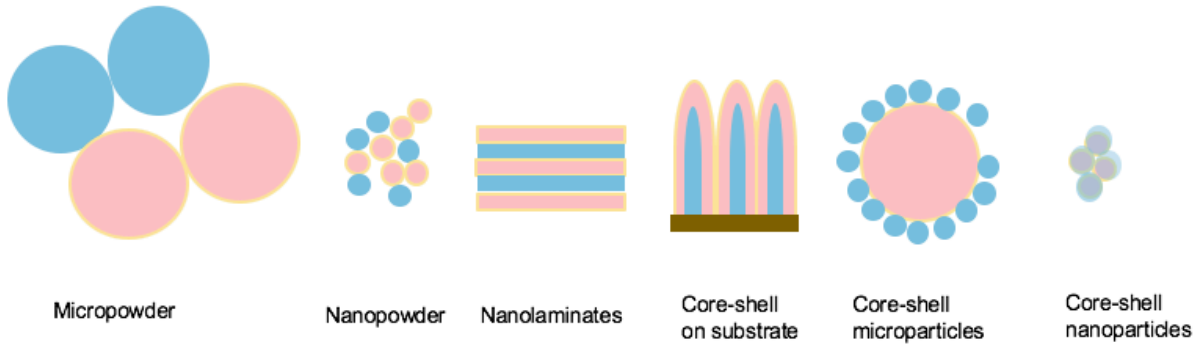

Figure2. 2 Comparison of different structures of thermites.

2.2 Types of thermites

There are various pairs of metal and oxide materials investigated for thermites, and they would have different features meeting various requirements. Common metal materials are aluminium, boron, zinc, silicon and magnesium. More types of oxide have been introduced into

this system, including Fe_2O_3, NiO, CuO, MoO_3 and WO_3, and the characteristic of the thermite reaction is highly material dependent. Table 1 compares the heat of reaction, adiabatic reaction temperature, state of products and gas production for thermites: Al/CuO, Mg/CuO, Al/Fe_2O_3 and Al/NiO. Even though Mg/CuO has higher energy release, Al is the more commonly used material, since Mg is more expensive, and Mg is sometimes too reactive. The oxide layer of Al_2O_3 outside of Al gives Al the advantage of stability and safety when compared to other highly reactive fuels. The heat flow traces of different Al-based thermites with a mixture of nano-powders are shown in Figure 2.3 and they are the major species of research interest in the past.[14]

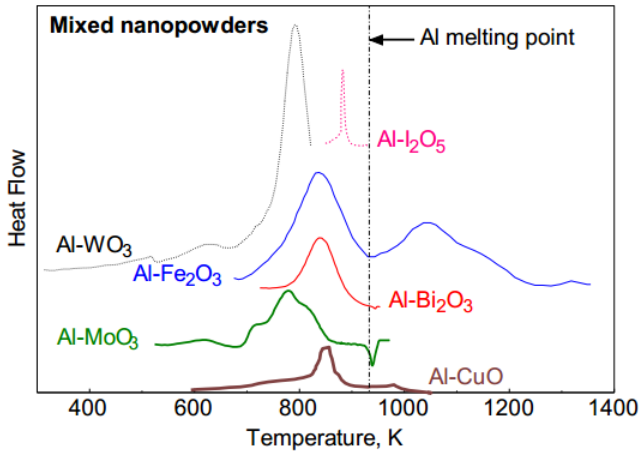

Figure2. 3 DSC traces for different thermites prepared with mixing of Al and oxidizer nanopowder[14]

Table 2- 1 Properties of selected thermites, modified from Fischer et al.[15]

Reactants	Heat of reaction (cal/g)	Adiabatic reaction temperature (K)	State of products		Gas production (gas / reactant)
			Oxide	metal	
2Al+3CuO	974.1	5718	liquid	l-g	0.3431
Mg+CuO	1102	6502	solid	l-g	0.5201
$2Al+Fe_2O_3$	945.4	4382	liquid	l-g	0.0784
2Al+3NiO	822.3	3968	liquid	l-g	0.0063

The amount of gas production by the material indicates the explosiveness of the material. If the material has a large amount of gas production, like Mg/CuO, it would be more suitable for producing explosives like fireworks, while it would not satisfy the welding or joining requirements, since too much bubble would be generated during the process. Al/CuO thermites have a relatively high-energy release and moderate amount of gas production, which makes them a well-studied type of thermite. Many theoretical and experimental studies have been conducted on the Al/CuO system, but the exact reaction mechanism behind has not been well explained since the thermite reaction involves many reactions, phase transformations and decompositions, which are shown below as equations, modified from Baijot et al.[16]

$$2\,CuO_{(s)} \leftrightarrow Cu_2O_{(s)} + \frac{1}{2}O_{2(g)} \quad \text{(Eq. 2-2)}$$

$$Cu_2O_{(s)} \rightarrow Cu_2O_{(l)} \quad \text{(Eq. 2-3)}$$

$$Cu_2O_{(l)} \leftrightarrow 2Cu_{(l)} + \frac{1}{2}O_{2(g)} \quad \text{(Eq. 2-4)}$$

$$Cu_{(s)} \rightarrow Cu_{(l)} \leftrightarrow Cu_{(g)} \quad \text{(Eq. 2-5)}$$

$$4Al_{(g)} + 3O_2 \rightarrow 2Al_2O_3 \quad \text{(Eq. 2-6)}$$

$$Al_{(s)} \xrightarrow{660\,℃} Al_{(l)} \leftrightarrow Al_{(g)} \quad \text{(Eq. 2-7)}$$

$$3CuO + 2Al \rightarrow 3Cu + Al_2O_3 \quad \text{(Eq. 2-8)}$$

Equation 2-2 shows the decomposition of CuO, which could be a reaction step before the thermite reaction. The phase change of Cu_2O is represented in equation 2-3 and it usually happens at 1232℃. Since the thermite reaction is fast and a huge amount of energy would be released during reaction, it is difficult to determine the phases of compositions. Equation 2-4 shows a further decomposition of Cu_2O and equation 2-5 shows the phase change of Cu. Equation 2-6 represents the combination of Al and O_2. The phase changes of Al are shown in equation 2-7 and this melting peak would be observed after thermite reaction in this series of experiments. Equation 2-8 represents the overall thermite reaction for Al and CuO.

Usually, thermite reaction for micro-composites appears after the melting of Al and the onset temperature is significantly affected by the particle size of Al,[17] while for micro-composites with core-shell structures, the onset temperature of thermite reaction could reduce to a temperature below the melting point of Al, indicating a condensed phase reaction for metal and oxide. Nano-thermites usually have advanced thermal properties when compared to micro-thermites, while the price of nano-particles remains high until now, besides the cost of the advanced machine to synthesise nano-thermites like the magnetron sputtering machine. The traditional application of thermites like pyrotechnics and munitions usually requires a large amount, so the product should be suitable for large-scale production with low costs and stability for transportation. Core-shell

spherical thermites with micro Al are developed for this purpose, whose thermal properties are similar to nano-powder thermites. Meanwhile, the core-shell spherical nano-thermites are investigated for more advanced applications like MEMS involving moving particles with higher requirements for the energy release. As mentioned previously, Al-CuO is a well-studied system in the last decade for all their promising properties, as a thermite and many different features of the material and the reaction have been well addressed, both theoretically and experimentally. We are introducing a relatively new structure with its advantages and drawbacks, and the reaction mechanism would be discussed as associated with the structure features.

2.3 Applications of thermites

Welding is the most important application for thermite material, due to the large amount of heat released, and the little amount of gas produced during thermite reaction. The thermite of the Al/Fe_2O_3 powder mixture has been applied in railway welding for a long time. During the welding procedures, molten Fe and Al_2O_3 would be produced and the iron would flow into the welding area due to the density difference and gravity. The application for thermites could be extended to underwater construction, such as wet welding and thermal drilling due to the zero-oxygen balance.[18]That feature makes thermites also suitable for welding in other low-oxygen or vacuum environments like spacecraft maintenance.

Propulsion and thrust is another popular direction for the application of thermites, since a large amount of heat would be produced and much gas would be generated for some types of thermites. For example, Gustavo et al. proposed a micro-actuator with elastic membrane, which could eject a few nano-litres of fluid under the high pressure generated by thermites; this micro-

actuator is suitable for a disposable lab-on-a-chip, as illustrated in Figure 2.4.[19] The application of thermites for the high-speed propulsion of underwater vehicles has been investigated by Hacker et al.[20] The gas generation and heat release for thermites could be well controlled by adjusting the structures and the compositions, so they could be utilised for the course correction of microsatellites, since they require a high precision of gas generation to avoid rotating.[21] Integrated with MEMs, many applications of thermites in biological areas have been developed, including intranuclear molecular transport and antimicrobial energetic systems.[22,23] Since the biological systems required precise control and low toxicity, thermites with specific compositions could meet these criteria.

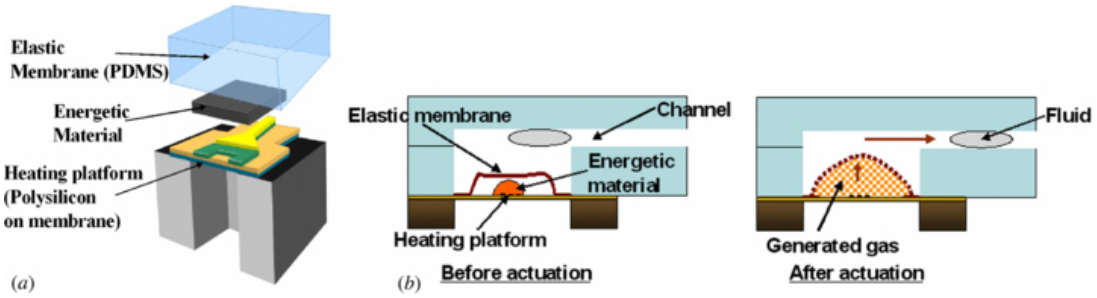

Figure2. 4 (a) 3D view of the structure of the micro-actuator. (b) Schematic of the working principle for micro-actuator from Gustavo et al.[19]

Thermites could also be used in metal refining, since the oxide will be reduced to corresponding metal during the thermite reaction. For instance, a Fe-Cr alloy will be heated with Na_2CO_3 and sulphur to form chromium oxide. Then, the oxide will be reduced to pure Cr by a thermite reaction.[24] While the products of oxide and metal could be hardly separated, this problem negatively impacts the promotion of thermites in metal refining. Moreover, the self-propagating thermite reaction could be utilized for melting of municipal solid waste incinerator fly ash. According to experimental results, fly ash of less than 30% in total mass of mixture with

thermites could start a self-propagating reaction and meanwhile, most of iron was retrieved as alloy while the rest of non-reductive oxides as slag.[25]

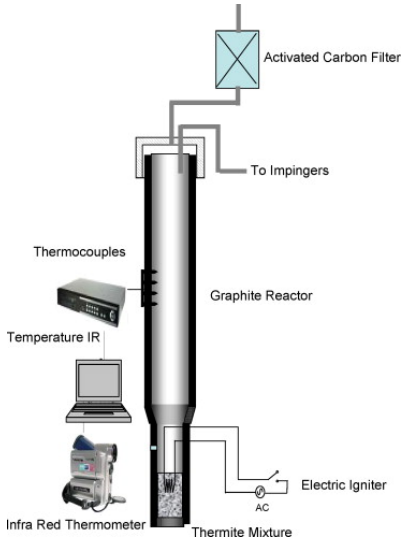

Figure2. 5 schematic of reactor for melting of municipal solid waste incinerator fly ash by waste-derived thermite reaction[25]

Thermites reaction will release a large amount of heat, while the thermite reaction also requires a high temperature and much energy to trigger, which limits the developments of thermites in portable and disposable devices. Jang et al. proposed an efficient assembly method of thermites with a polymeric lens, which could be ignited by a remote low-power pointer with a low input power of about 500 mW.[26] As shown in Figure 2.6, a thin polydimethylsiloxane membrane can be incorporated with the optical igniter containing thermites to form a pressure-driven membrane actuator, which is reproducible and cost-efficient. Thermites with these new ignition techniques could be applied in smaller devices with microheaters, and the consistency and controllability of laser ignition further improve the controllability of nano-thermites.

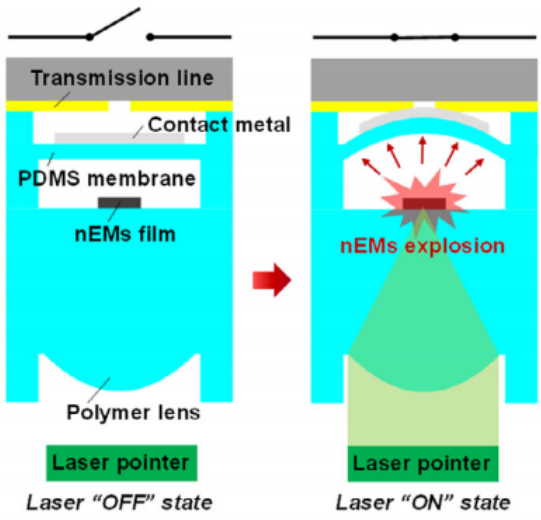

Figure2. 6 The working principle of alarm switch operated remotely using a focused-laser-assisted igniter from Nam-su et al.[26]

2.4 Fabrication methods of thermite composites

Thermites have been utilised for hundreds of years and various methods have been developed to fabricate better thermites with different features. Popular methodology includes arrested reactive milling[27], vacuum filtration[28], electrophoretic deposition (EPD)[29], electrospraying[30], atomic layer deposition[31], sputtering[32,33,34], sol-gel synthesis[35,36], DNA-directed assembly[37] and sonication[38,39]. As mentioned previously, the reaction rate and energy release of thermites are dependent on the transfer efficiency of heat and mass, as well as the degree of contact between fuel and oxide. Researchers tried many methods to increase the interfacial contact between reactants, which in turn facilitates the diffusion between them and increases the rate of energy release.[40] The features of different methodologies will be discussed below, and they are divided into particles and layered structures.

Both sonication and ball milling belong to physical mixing, which should be the simplest method to prepare composites. In sonication, two types of particles would be dispersed in a solvent and be ultrasonicated in a bath to reduce agglomeration. Organic solvents like ethanol and hexane are usually used for their poor reactivity with Al and low evaporation temperature. Sonication would not change the feature or size of the reactant particle, while ball milling usually reduces the particle size, since the strong motion between grinding balls and reactants. For sonication, metal and oxidiser particles usually have different velocities during sonication, making it difficult to produce homogeneous mixtures. One major disadvantage of the ball milling method is that the impact of motion is possible to ignite the thermite, which is a serious potential safety problem. For large-scale production, this method is not recommended. Different morphologies of samples prepared by arrested reactive milling with different milling durations are shown in Figure 2.7.

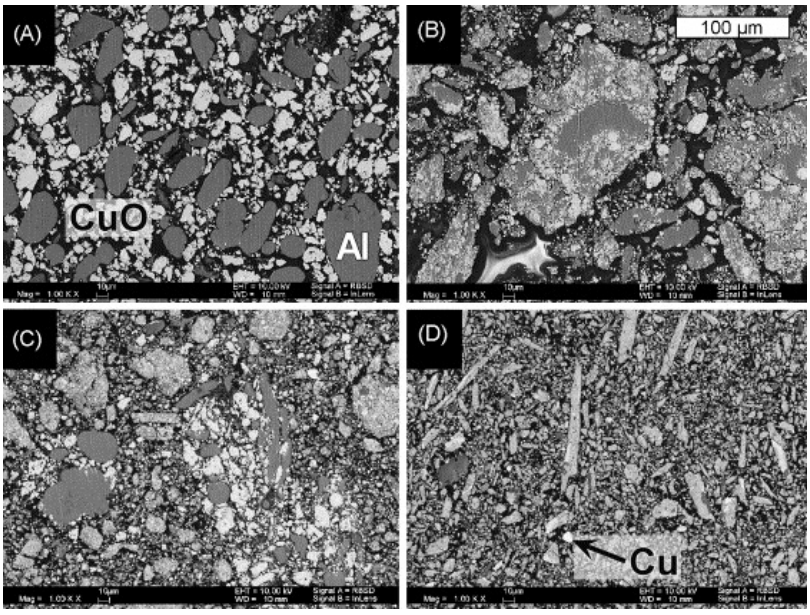

Figure2. 7 SEM image of Al/CuO synthesize by arrested reactive milling with different milling durations and different morphology of the samples by Umbrajkar et al.[27]

The sol-gel method is another widely used way to create a more homogeneous structure of components. During processing, the salts of metal would be dissolved in ethanol to form a solution, which is called sol. Then, propylene oxide would be added in to condense the sol to form a porous structure, which is called gel, and fuel particles could be mixed with gel to create direct contact with porous structure. Finally, the fluid in the pores could be removed by exvaporation.[41] Compared to other methods, sol-gel processing offers an inexpensive method of generating a shorter diffusion distance between two reactants and an increased reaction rate, though there are some impurities as a result of the introduction of polymer. Meanwhile, the sol-gel processing is restricted by the species of hydrated salts, since some of those salts could not be gelled, which limits the application of this method. Moreover, the time of the addition of metal particles influences the final product, which affects the stability of this method.

The self-assembly method has been developed based on sol-gel method, which generates a more ordered structure compared to the sol-gel method. The precursor material would be hydrated metal salt again or oxide rod, which would be functionalised by polymers. The introduced Al particles could adhere the surface of oxide to generate direct contact. If the metal salt is applied, the processing procedures are similar to those of the sol-gel method to reach the condensation phase and the difference lies in the functionalisation process, which also provides a more ordered structure.[42] Moreover, there is no specific requirement for the stage of addition of metal particles, since Al would be adhered on the surface of oxide with the functionalisation step. This method improves the stability of the sol-gel method and the final product would be better distributed and ordered. The drawback of this method is the high cost of the modified oxidiser. There is a schematic of self-assembly method procedures given in Figure 2.8.

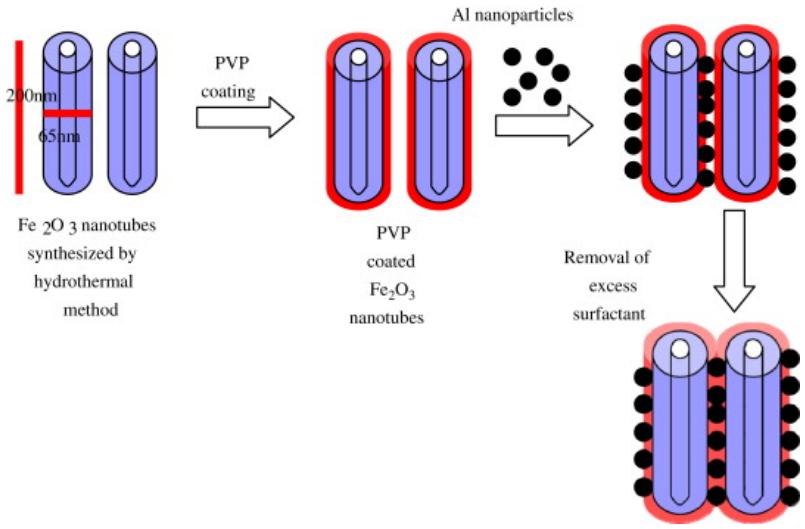

Figure2. 8 Process of self-assembly synthesis of Al/Fe_2O_3 thermite, from Cheng, *et al*.[42]

There is one popular synthesis method for the core-shell structure integrated with deposition and oxidation. First, one 100-nm thick SiO_2 would be coated on top of the glass as buffer layer and one Ta film with thickness of 50 nm would be deposited by the radio frequency sputtering as an adhesive layer. Then, Cu thin film would be deposited as well and Cu films would be cleaned by HCl and de-ionised water, before being oxidised in air at 500°C. Al would be deposited by RF sputtering or magnetron sputtering after the natural cooling procedures of CuO to prevent it from peeling-off.[43,44] The contact area between CuO and Al produced from this method was increased and many voids generated by physical mixing could be prevented. According to SEM results, the CuO nano-wires are fully covered by Al deposition, so the burning rate and reaction rate could be improved through this method. The synthesis procedures and corresponding SEM images of Al/CuO nano-wires are shown in Figure 2.9. The high homogeneity of the product provides promising reactivity and the heat release was higher than that of nano-power mixing products.

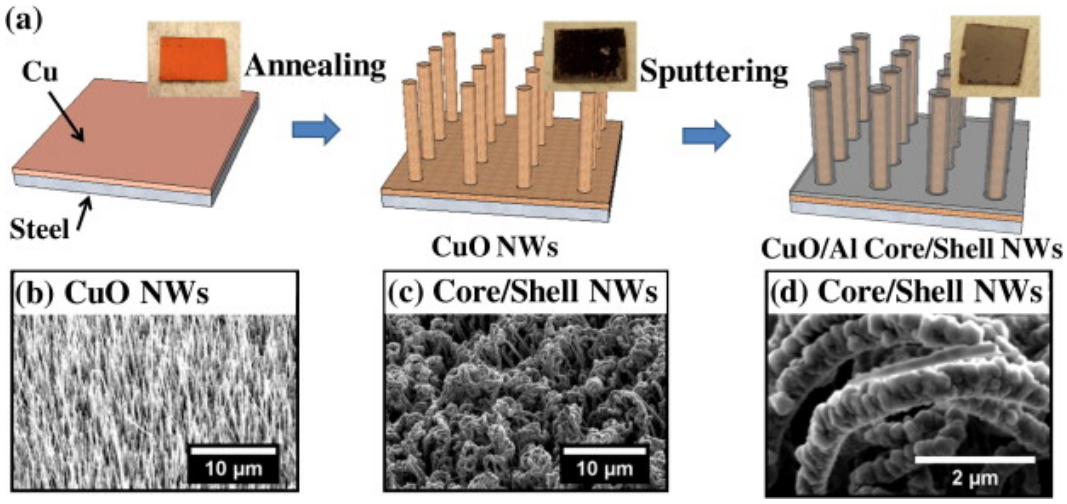

Figure2. 9 Schematics of the fabrication process of the CuO/Al core/shell NWs and the corresponding SEM images by Ohkura et al .[44]

Many thermites with layered structure have been developed in recent decades for their even larger contact area between reactants. Moreover, the characteristics of layered structures could be controlled through different thickness and consequences of metal and oxide layers to meet specific requirements. Multi-layered samples are also a suitable tool to study the reaction mechanism and ignition characteristics of thermites for their promising stability.[45] Also, layered structure thermites could meet some specific requirements, like a tailored burning rate for propellant.[46] There are several different methods to create layered structures, including electrophoretic deposition, vacuum filtration, magnetron sputtering and atomic layer deposition. For electrophoretic deposition and vacuum filtration, each layer contains the reagent particles and the contact area of metal and oxide is relatively large. The advantages of these two methods are the potential for large-scale production and low cost, while the layer generated by these methods is not very uniform, which would influence the thermal properties of the thermites. Moreover, limited materials could be utilised in the EPD method, since it must be able to be discharged in suspension. The layered

structure of product by EPD method is shown as below and the layer structure is uniform.

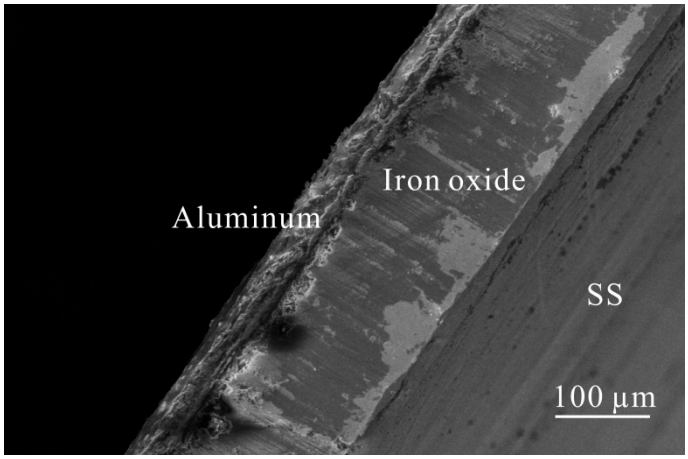

Figure2. 10 SEM image of the cross-section view of layered Al/Fe_2O_3 composite by Sui, *et al.*[29]

Atomic layer deposition, electron beam evaporation and magnetron sputtering would produce more uniform and thin layers for higher homogeneity. ALD involves deposition of a gas phase oxide material (like Co_3O_4)[47], NiO[48] on a substrate and that material would react with the substrate in order to generate a layer on top of the substrate. It increased the uniformity of the layer structure and the thickness would be better controlled, while the high temperature environment (250℃-350℃) in this deposition would sometimes initiate the thermite reaction, which is dangerous. Additionally, the reaction involved in the synthesis procedures will introduce some impurities into the system. For example, the synthesis of SnO_2/Al nanolaminates via atomic layer deposition would produce HCl, which could react with the passivation layer of Al_2O_3 and influence the thermite reaction consequently.[49]

Electron beam evaporation was utilised to produce multi-layered thermites previously, while the surface roughness of each layer would influence the number of layers that would be consumed during reaction, and the homogeneity of products is not promising.[50] Later, sputtering methods attract more attention due to the higher homogeneity and better efficiency in deposition. For the sputtering method, the ejected target material would be partially ionised first, fly and impact on the substrates. It is also possible that those ions collide with the gas to create positively ionised gas, which bombards the target and condenses on the substrate. The substrate would be rotating during deposition process for a better quality, and argon is commonly used in the gas environment since it is inert and heavy enough. The product with a layered structure prepared by sputtering is shown in Figure 2.11, and the layers could be very thin and uniform. Sometimes, oxygen is also used as the gas source to oxidise metal to create metal oxide layers on the substrate. When compared to other methods, the layered structures produced by sputtering method offer a much better controllability of the layer thickness and consequences, leading to precisely tunable thermal properties. Meanwhile, the simple geometry and well-defined processing makes products stable and easy to model. However, the specific conditions required for deposition make it difficult for this type of material for large-scale production, and the Al layer without passivation layer which is less than 100nm could lead to a spontaneous thermite reaction.[33]

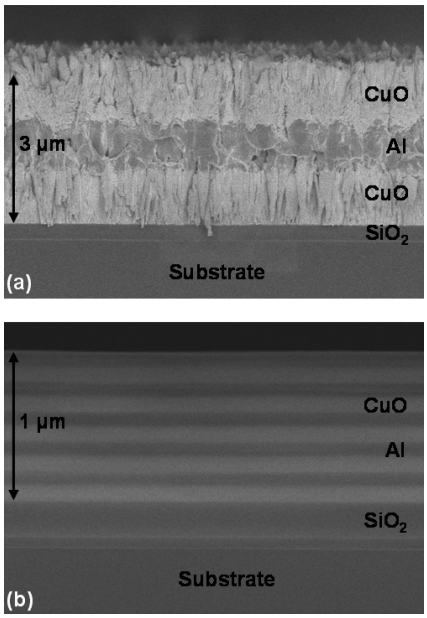

Figure2. 11 SEM cross-section images of multilayers magnetron sputtered. A: 3 layers CuO(1 µm)/Al(1 µm)/CuO(1 µm). B: 10 layers of CuO(100 nm)/Al(100 nm).[33]

Table 2.2 below compares some features of physical mixing, arrested reactive mixing, sol-gel, self-assembly, electrophoretic deposition and magnetron sputtering methods. Among them, sputtering methods could produce multi-layer or core-shell nanowire structures with extraordinary thermal performance and the lowest level of impurity, while the high-power source required to create the plasma in magnetron sputtering and expensive target material limit the scalability of this method. Moreover, the ultra-thin layers created by sputtering without a passivation layer may lead to an in-situ reaction. The products of sputtering and electrophoretic deposition are not free-standing, and the existence of substrate also sometimes affects the application negatively. Arrested reactive mixing could create more uniform products when compared to physical mixing, while the thermite reaction could happen during the preparation duration due to high temperature and milling collision. Sol-gel and self-assembly methods produce more homogeneous products with a high contact area and low cost, while relatively more impurities would be introduced to the system and

synthesis is sometimes limited by the species of raw material.

Table 2- 2 Comparison of preparation methods discussed in this chapter of the structure formed, cost, scalability, impurity level and safety

Synthesis method	Structure formed	Cost	Scalability	Impurities	Safety
Physical mixing	Powder	Low	Easy	Low	Safe
Arrested reactive mixing	Powder	Low	Not easy	Low	Dangerous
Sol-gel	Monolithic bulk	Low	Easy	High	Precaution needed
Self-assembly	Monolithic bulk	Relatively low	Easy	High	Concern
Electrophoretic deposition	Thin film	Low	Easy	Low	Safe
Magnetron sputtering	Multi-layer/core-shell nanowire	High	Difficult	Very low	Usually safe

2.5 Review of thermite reaction of Al with CuO

For the reaction between Al and oxygen, oxygen diffuses through the passivation layer of Al and reacts with Al when the temperature is below the melting point of Al (~660℃), which is solid-gas reaction. When the temperature exceeds the melting point of Al, the molten Al diffuses outside and reacts with oxygen, leading to a liquid-gas reaction. While for the reaction between Al and CuO, it is possible that they react before the melting point of Al, and the reaction is a solid-

solid reaction. So far, it is not clear if the oxidiser would decompose before or during the reaction. The reaction mechanisms influence the thermal properties in combustion propagation and gas production, and correspondingly determine the application direction. There are several important parameters regarding to thermite reaction when the reaction is described, including onset temperature, peak temperature, average energy release, activation energy and ignition delay.[51]

It is challenging to obtain a thorough understanding of the reaction mechanisms of micro-composites and nanocomposites, since different reaction mechanisms could exist together. When sufficient energy is introduced into the system, the thermite would have a self-sustained flame propagation and the heat rate of self-sustained reaction could only be roughly estimated, which is about 10^4-10^8K/s.[52] It is critical to simulate that environment and reach the same heat rate in any device. Moreover, the moment of triggering ignition could only be captured by a high-speed camera. So differential scanning calorimetry (DSC) is utilised to module the natural ignition environment to study the thermal properties in a lot of cases. Laser ignition with an even higher heating rate up to 10^6-10^7K/s was used to investigate the ignition characteristics of thermites, during which the data of optical signals would be collected by a high-speed camera and thermocouples.[54] The shock tube has been used to study the combustion properties as well, and the heating rate of this method could reach 10^5-10^6 K/s. A schematic of shock tube measurement for thermite ignition is shown in Figure 3.1.[53]

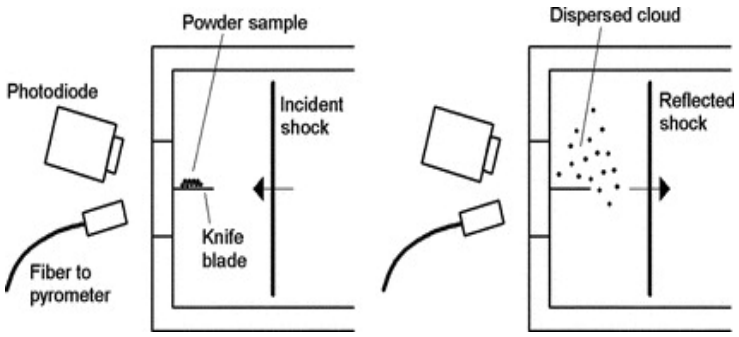

Figure2. 12 A schematic of the shock tube experiments. Left: Prior to arrival of the incident shock at the endwall. Right: After shock reflection.[53]

Onset temperature refers to the temperature where it is assumed that the significant consumption of fuel starts and it is also called ignition temperature.[51] In DSC studies, this temperature is where the exothermic thermite reaction begins and it is influenced by heating rates, particle size and pressure. Ignition delay is another feature commonly used to describe the characteristics of thermites and it could be defined differently depending on the ignition system. Generally, the time interval between the starting moment of heating and the beginning of the thermite reaction is the ignition delay. In laser ignition, it could be considered as the interval between the moment when laser reaches the sample and the moment of light emission from the sample. For nano-thermites, both onset temperatures and ignition delay would decrease compared micro-thermites under same conditions and that is important for applications in micro-thrusters and munition primers.

For most thermites, the thermite reaction is self-sustaining, where the energy released would be transferred to the local area and ignite the next one. Four propagation mechanisms are possibly involved in heat transformation: thermal conduction, convection, radiation, acoustic/compaction. Acoustic/compaction is related to detonations and is not particularly related

to thermites.[52] It is possible that radiation contributes to the energy transformation, but it should be a small proportion compared to other mechanisms.[55] In order to investigate the function of convection in thermite reactions, both loose powder and packed powder samples of Al/CuO, Al/WO_3, Al/MoO_3 and Al/Bi_2O_3 were measured, and the propagation rate of the packed sample was decreased.[56] It is considered that the convection flame propagation mechanism is dominant in the energy transformation in low density samples.

2.6 Characterization methods

2.6.1 Thermogravimetric Analysis (TGA)/Differential Scanning Calorimetry

TGA provides thermal analysis during which the mass of the sample is measured over time with temperature changing. The change in mass with temperature could be explained by physical phenomena including absorption and phase transitions, or chemical phenomena such as thermal decomposition and oxidation. In this thesis, TGA is a useful tool to determine if the sample is fully oxidized since the release of gas of not fully oxidized sample leads to a drop in mass. Additionally, it is important to measure the active contents of Al since as-purchased Al particles own the Al_2O_3 layer originally. The amount of Al_2O_3 could be calculated through the increased mass when Al particles is heated under oxygen flow.

DSC measures the difference in the amount of energy required to increase the temperature in the machine environment of a sample with the empty reference crucible. When there is a reaction or a phase transition, the difference in energy required indicates amount of energy absorbed or

released by the sample. DSC collects the heat flow information and offers the quantitative information on thermite ignition temperature, energy release and activation energy. In this thesis, a NETZSCH STA 449 F3 Jupiter machine, as shown in Figure 3.2 is used to measure the properties combining NETZSCH Proteus Thermal analysis software for data analysis.

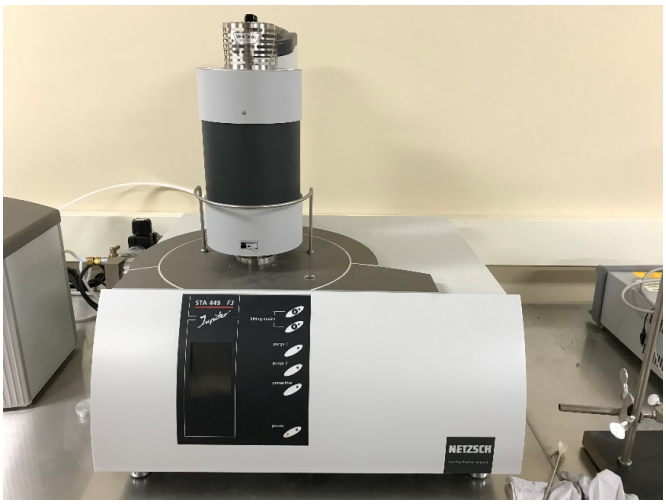

Figure2. 13 the NETZSCH STA 449 F3 Jupiter DSC machine used for this thesis

2.6.2 X-Ray Diffraction (XRD)

X-ray diffraction (XRD) is a commonly used technique to investigate the crystal structures and atomic spacing of material, which is based on constructive interference of X-rays and the sample. The interaction of X-rays with the sample produces constructive interference and a diffracted ray when conditions satisfy Bragg's Law:

$$n\lambda=2d\sin\theta$$

where λ is the incident X-ray wavelength, d is the planar spacing of the element and θ refers to the incident angle. All possible diffraction patterns of the lattice would be obtained through various

angles of the sample are scanned since the sample is in form of powder. The diffracted X-rays and different intensities of peaks would be recorded by the detector. The d-spacing could be calculated with values of λ and θ and it corresponds to different types of material.

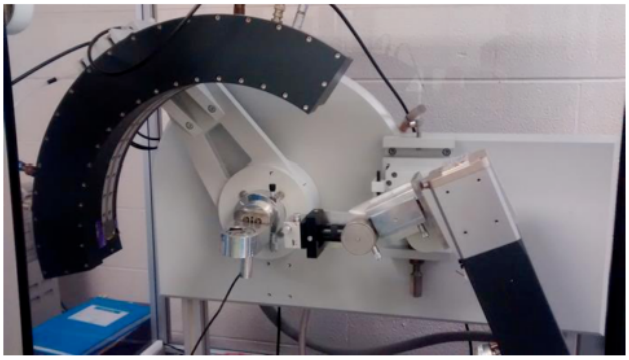

Figure2. 14 INEL Powder X-ray Diffractometer

2.6.3 Scanning Electron Microscopy /Energy Dispersive X-ray Spectrometer

Scanning Electron Microscopy (SEM) is a useful tool to capture high resolution image of sample down to micro- and nano- scale with details of surface morphology and elemental contrast. In SEM, the sample would be scanned by a focused electron beam and the atoms in the sample would react with electrons, resulting in various signals. There are two main types of electron beam, secondary electron beam with relatively low energy and back-scattered electron beam. In this thesis, SEM is utilized to observe the surface morphology of particles and estimate the coating quality roughly. Successfully coated and unsuccessfully coated samples can be compared with the help of SEM combined with EDS due to the elemental contrast. The structures of samples after reaction were also measured in SEM to obtain a more reliable understanding of the thermite reaction of this sample. For this thesis, a Zeiss field emission SEM with EDS was used.

Energy-dispersive X-ray spectroscopy (EDS) is an analytical tool commonly used for the elemental analysis of a sample. In EDS, X-rays would be focused on the sample and the incident beam would excite an electron with lower energy, then an electron from higher energy would fill the left hole. The energy difference between these two electrons would be released in a form of X-ray and those X-rays would be measured by an energy-dispersive spectrometer, which provides both identity and rough quantity of different elements. Since the accuracy of the quantitative analysis is related to the composition, the density of the sample, the quantitative analysis of EDS could only be used as a reference. In this thesis, EDS provides elemental information combined with the surface morphology of SEM to show the distribution of different elements throughout the particles. Samples before and after thermite reactions were measured for elemental distribution, and further discussion of reaction mechanisms could be obtained through the change of elemental distributions.

2.6.4 X-ray Photoelectron Spectroscopy (XPS)

X-ray photoelectron spectroscopy (XPS) is a useful tool for measurement of elemental composition within 20nm of the surface of the sample. Chemical state, electronic state and empirical formula would be obtained through XPS. Generally, XPS shows the existence of the element and the other elements that it bonds to. When a beam of X-rays is applied to a material, the kinetic energy and the number of electrons escaped would be recorded and analyzed. In this thesis, XPS is used to distinguish the oxidation state of Cu and determine the degree of oxidation during synthesis of Cu. A Thermo Scientific ESCALAB 250 was used for this thesis.

2.6.5 Transmission electron microscopy (TEM)

Transmission electron microscopy is a useful microscopy technique to observe the surface morphology of the sample. In TEM, a beam of electrons would be transmitted through the sample and the interactions of the electrons with the sample would form a high-resolution image. For the sample preparation, the powder sample would have to be placed in ultrasonic devices for several minutes to break the agglomeration of particles and a small droplet of the suspension on the grid would be enough for measurement since the electrons need to be transmitted through the particles. The magnified image of TEM result could give fine detailed analysis on the structure and it is very useful in nanocomposites analysis.

2.6.6 High speed camera and Photodiode

A high-speed camera was utilized to record the laser induced ignition of the thermite along with the Photron FASTCAM Viewer software (3.6.9.1). The ignition delay could be counted as the difference between the moment that laser hits the thermite and the moment that the thermite reaction starts. The initial flame propagation speed of the reaction could be calculated through the video as well. An Osram SFH206K photodiode (1 ns response time) was integrated with laser ignition setup and the ignition delay and energy release of the sample would be recorded. The signals of illumination and thermite reactions would be emitted by the photodiode, whose difference is regarded as the ignition delay. Meanwhile, the normalized time-averaged photodiode signal term represents the specific energy release rate by the reaction.

3.0 Experimental

3.1 Synthesis methods

Al powders with an average diameter of 1μm and 40nm used in this work were purchased from US Research Nanomaterials Inc. The elemental contents were 97% of Al by weight and 3% of Al_2O_3 for Al particles with diameter of 1μm. For Al particles with a diameter of 40nm, the active content is about 67.5% of the total mass. Acetone, ethanol, ammonia hydroxide solution and cupric nitrate ($Cu(NO_3)_2 \cdot 2.5H_2O$) were used as received from Sigma Aldrich. Synthesis of Al/CuO particles with a core-shell structure is illustrated in Figure 1. The synthesis included two steps: 1) hydrolysis; and 2) thermal decomposition. Cupric nitrate was used as the precursor for copper oxide. 0.5g Al powders were placed in 100ml ethanol and the suspension was stirred at a speed of 250 rpm for 10 minutes. Then, a mixture of 1g $Cu(NO_3)_2 \cdot 2.5H_2O$, 2mL aqueous ammonium hydroxide (NH_4OH, 15%) and 10ml ethanol was added into the Al suspension, and stirred for four hours. The colour of the suspension would turn to blue grey from grey. The shell composing of $[Cu(NH4)]^{2+}$ and OH^- was formed on the Al particle through the electrostatic force. The core-shell particles were collected by vacuum filtration using a piece of filter paper (Whattman, grade 42). A 140-mesh sieve was used to break down the aggregated particles after the vacuum filtration. The collected particles were then heated up to 250℃ for two hours in air. They were ground to pass the sieve again to break the agglomerates. The colour of the products was dark grey, indicating the formation of CuO. In addition, a reference group of mixed Al powders and 40nm CuO powders was prepared with the same equivalence ratio of three to compare the energy release. Al powders and CuO powders were added into ethanol and sonicated for 120 minutes. The mixture was then collected through the vacuum filtration and heated to 100℃ to remove the ethanol and they were ground to pass the sieve to reduce the agglomerates.

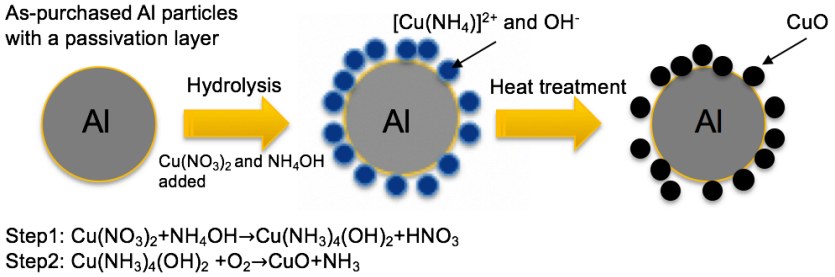

Figure3. 1 Schematic of synthesis procedure of Al/CuO micro-particles with a core-shell structure.

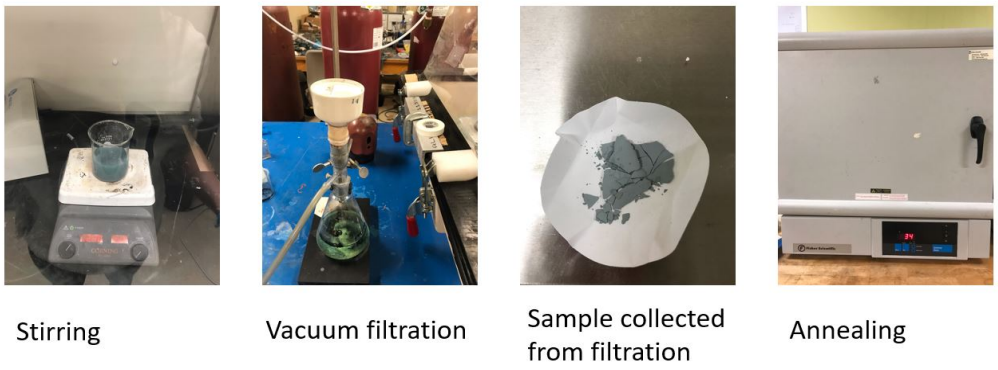

Figure3. 2 Experimental procedures of synthesis of the samples

The stoichiometric thermite reaction is $2Al + 3CuO \rightarrow Al_2O_3 + 3Cu$. The equivalence ratio was used to investigate the energy release, which is defined as the molar ratio of the fuel agent to the oxidizing agent used in real cases divided by that of the stoichiometric reaction, as shown in the following equation:

$$\Phi = \frac{(^{Fuel}/_{Oxidizer})_{real}}{(^{Fuel}/_{Oxidizer})_{stoichiometric}} \quad \text{(Eq3-1)}$$

The equivalence ratios of 5, 3 and 1 (denoted as sample 1, sample 2, and sample 3 in this paper) were used. Loss of Al, Cu complex and CuO during the vacuum filtration and grounding was

assumed not to affect the equivalence ratios. The reference sample would be prepared by ultrasonic mixing for 2 hours and they would be collected by vacuum filtration and drying as well.

3.2 Determination of the composition and structure of the Al/CuO microparticles

During stirring, $[Cu(NH4)]^{2+}$ ion and OH^- ion would combine to form a condensed layer around the Al core, driven by the electrostatic force, which would be further oxidized to CuO after annealing. As seen from Fig. 3.2 (a), two major types of peaks correspond to Cu complex and Al before annealing. After annealing, the XRD spectrum in Fig. 3.2 (b) of prepared samples exhibits dominant peaks of Al and CuO suggesting the oxidation of Cu complex. For samples after DSC measurement up to 900℃ shown in Fig. 3.2 (c), all of CuO would be reduced to Cu and Al_2O_3 forms at the same time. The change in the sample composition confirms the occurrence of the thermite reaction between Al and CuO and we could see some Al left after reaction, which matches the melting peak of Al in DSC curves. The alloy Al_2Cu is also formed during the reaction, which might influence the energy release performance of the thermite. The composition of the sample is further confirmed by X-ray photoelectron spectroscopy (XPS), which is a surface-sensitive quantitative technique and measures the elemental composition at counts per second. As shown in Fig. 3.3 (a), both elemental signals of $Al_{2p3/2}$ in Al and Al_2O_3 exist and the signal of $Al_{2p3/2}$ in Al_2O_3 is stronger than that of Al, because the probe of XPS works within 30nm of the surface and passivation layer of Al_2O_3 together with CuO layer cover the majority of the particle surface. Only a small proportion of Al could be detected by XPS. From Fig. 3.3(b), the oxidation state of Cu could be confirmed and they are all oxidized to CuO.

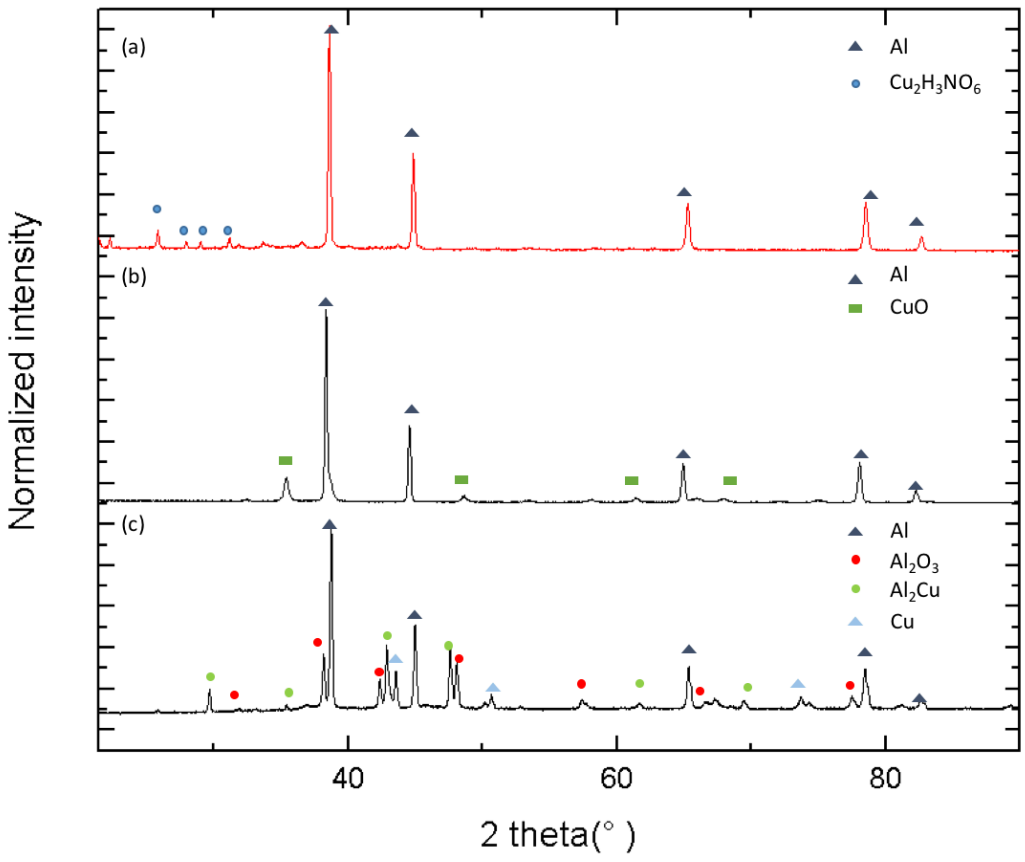

Figure3. 3 XRD spectra of the sample during fabrication: (a) before and (b) after annealing. The sample after reactions with the DSC test: (c).

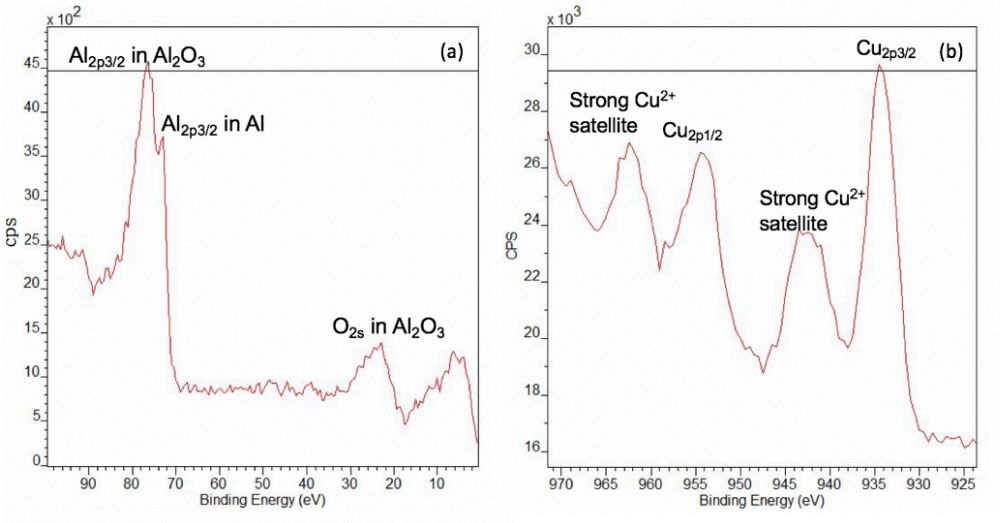

Figure3. 4 XPS spectra of the sample: (a) feature peaks of Al, (b) feature peaks of Cu

On the as-purchased Al micro-particles, there is a passivation layer of Al_2O_3 around the Al core, as shown in Fig. 3.4 (c). The thickness of this layer for Al particles with diameter of 1μm is about 10-20 nm. On these core-shell particles fabricated in this study, the newly formed CuO shell is distinguishable by contrast in Fig. 3.4 (a) and 3.4 (b), which has a various thickness of from 70-100 nm. This thickness is however not constant over the entire surface of the Al micro-particles, resulting from the nucleation and growth of CuO from both solution and annealing. The coating morphology including surface coverage and adhesive agglomerates, as shown in Fig.3.4 (a). Since the accelerating voltage of this TEM image is 200 kV, the electron beam is able to penetrate through the particle and reveals the overall composition of this particle. Fig. 3.5 (c) located the core Al and Fig. 3.5 (d) shows the distribution of Cu.

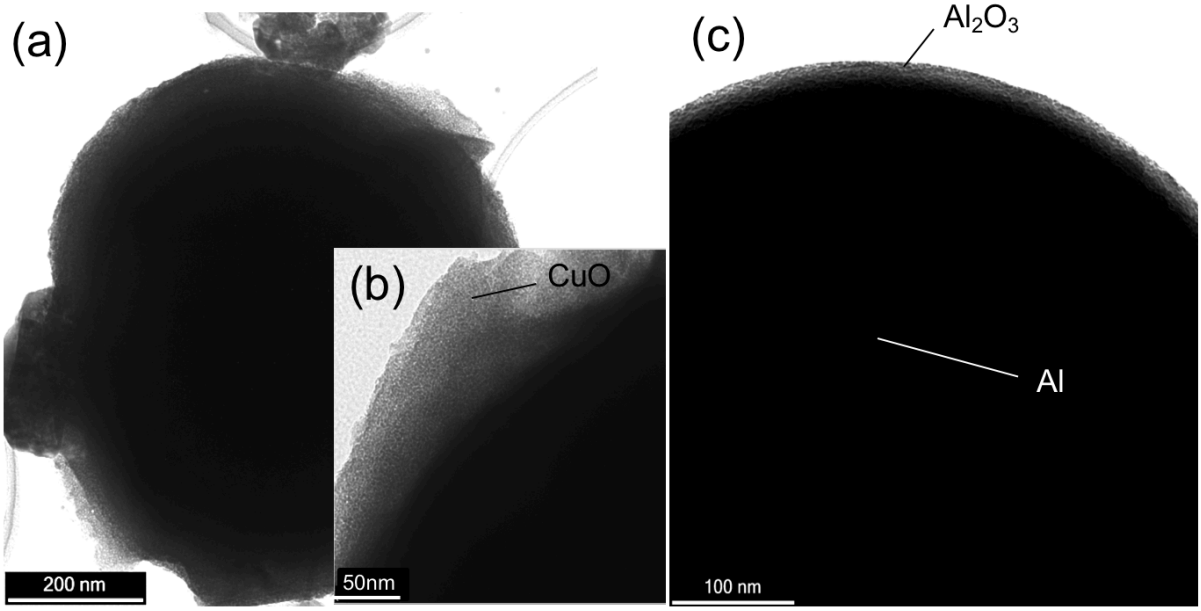

Figure3. 5 TEM images of (a) as-fabricated Al/CuO core-shell micro-particle; (b) enlarged edge of the as-fabricated micro-particle; and (c) as-purchased Al micro-particle with a passivation layer.

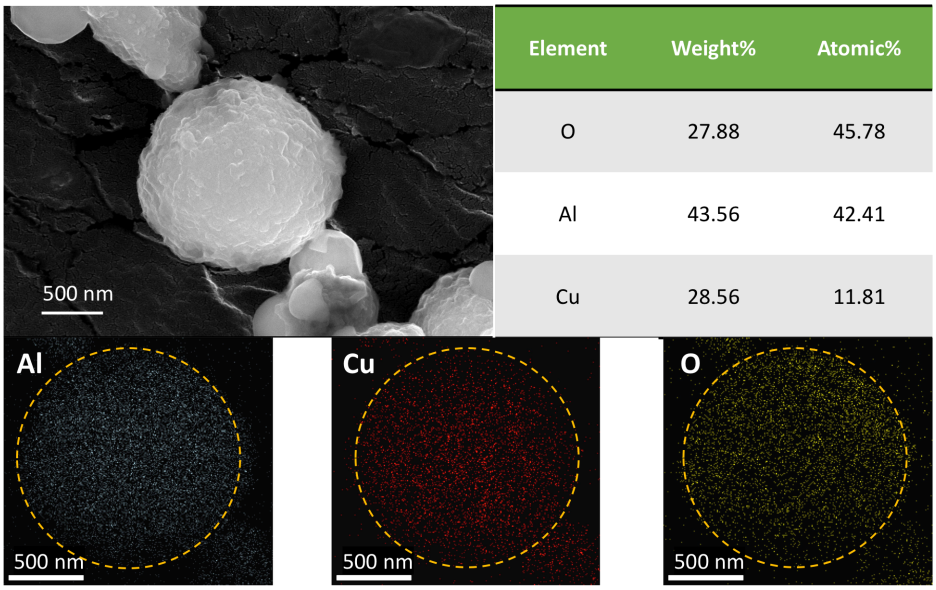

Element	Weight%	Atomic%
O	27.88	45.78
Al	43.56	42.41
Cu	28.56	11.81

Figure3. 6 (a) TEM image of the sample, (b) EDS mapping result of the particle, (c) EDS mapping result of Al and (d) EDS mapping of Cu

As shown in Fig. 3.6 (a), both successfully and unsuccessfully coated micro-particles indeed exist in these samples, due to the limitations of the solution phase synthesis. In this figure, these two-connected particles, sized with 1μm and 400 nm, respectively, located on the left side of the figure are nearly fully covered by a layer of CuO structures formed from the synthesis, while the nearly bare Al particle, sized with 850 nm, is not fully coated. Note that both types of micro-particles have a cluster of smaller CuO particles sticking on their surfaces. In addition, the elemental mapping images in Fig. 3.6 (b) and (c) illustrate the different amounts of CuO in the successfully coated sample and unsuccessfully coated sample. Some finer CuO nanoparticles also distribute away from the original Al micro-particles.

The observed characteristics of the microstructure of the core-shell micro-particles help to reveal the reactions between the Al core and the CuO shell. In ambient, the as-fabricated micro-particles contain an amorphous layer of Al_2O_3 between the Al core and the CuO shell, which prevents any chemical reactions between Al and CuO and makes the system metastable. The initial stage of the reaction would be explained by Cabrera-Mott oxidation mechanism, where the amorphous Al_2O_3 grow and the growth layer is limited by the outward diffusion of aluminum cations.[57,58] There is a critical thickness for the growth of Al_2O_3, which is determined by the crystallographic orientation of aluminum and temperature. The amorphous Al_2O_3 would start to transition γ- Al_2O_3 when the critical thickness is reached.[57] When the onset temperature of the thermite reaction between the Al core and the CuO shell is reached, active species including oxygen and metal ion will diffuse through the Al_2O_3 shell. Subsequently, the CuO shell will be reduced to Cu, while Al is oxidized into Al_2O_3. The thermite reaction propagates across the micro-particle, until one of the reactants (CuO or Al) is consumed. Diffusion of reactive species through the Al_2O_3 shell is similar to that happening during the condensed phase oxidation between metal oxide and Al nanoparticles.[59] This mechanism is different from other structures such as multiple nano-layers of CuO and Al which possess a heterogeneous reaction.[60,10] For the thermite reaction within the produced core-shell micro-particles, their microstructures facilitate a large contact area between Al and CuO and a short diffusion distance for active species. Condensed phase reaction is likely to initiate and sustain the interested thermite reaction.

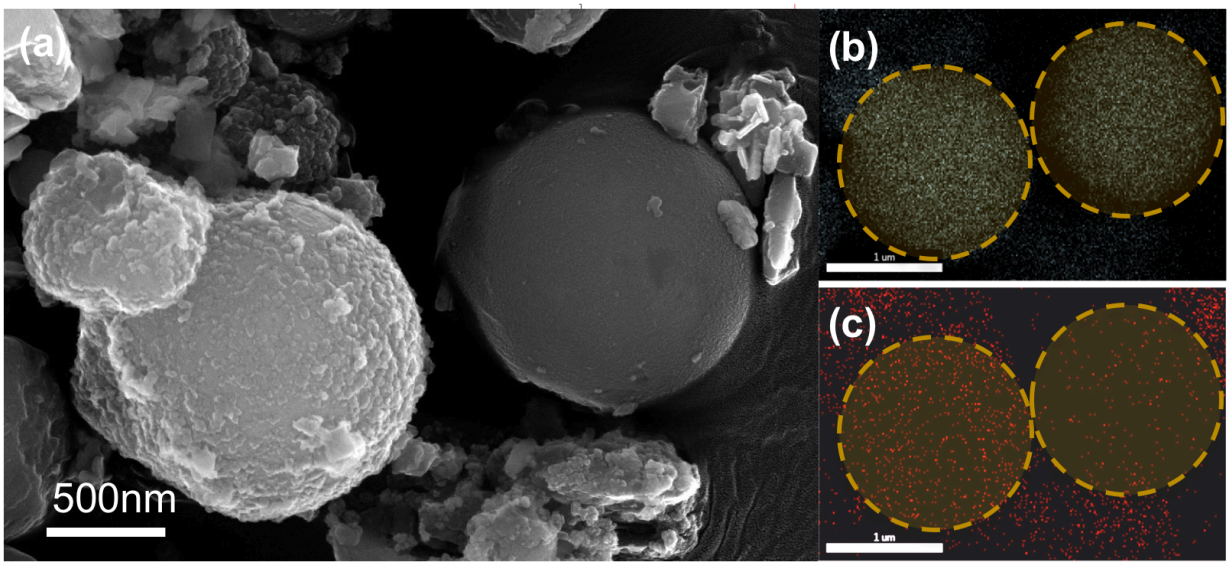

Figure3. 7 (a) SEM image of as-fabricated Al/CuO sample; (b) and (c): EDAX elemental mapping of Al and Cu, respectively.

3.3 Determination of the composition and structures of Al/CuO nanoparticles

The synthesis of Al/CuO nanoparticles follow the same synthesis procedures but the intrinsic features of nanoparticles cause a difference in coating result and the compositions after reaction. The XRD result of the sample at different stages are shown as the Fig. 3.7. After annealing, CuO are formed with the existence of Al. After the DSC measurement ending at 800℃ under argon, Sample in Fig. 3.7 (b) contain both Cu and Cu_2O, along with Al and Al_2O_3. These phases illustrate that the exothermic reaction has

not completed at this point and the formation of Cu_2O confirmed that CuO would be reduced to Cu_2O first, followed by further reduction of Cu_2O. Sample from Fig.3.7 (c) shows the composition after DSC measurement ending at 1200℃. All of Al and Cu_2O have been consumed indicating a fully reacted thermite reaction since the equivalence ratio of this sample is 1. And one composite

material formed during this high-temperature process. It has been reported that ceramic crystal materials like Al_2O_3 surrounded by Cu matrix under oxidant conditions could form a ternary phases of the system Al-Cu-O, the spinel Al_2CuO_4.

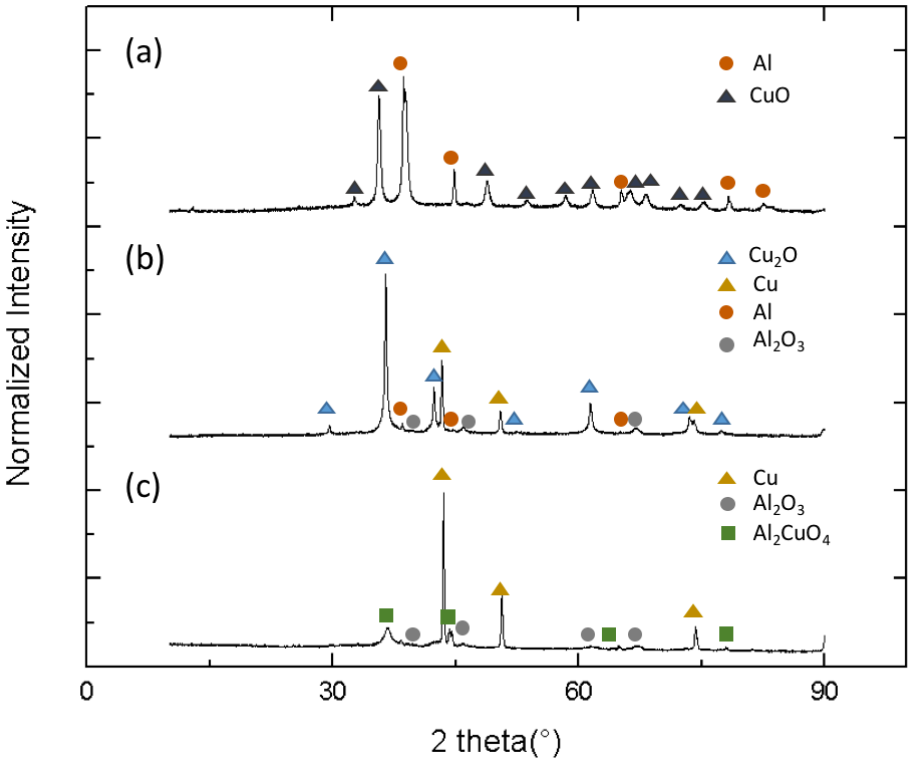

Figure3. 8 XRD results of sample1 with equivalence ratio of 1: (a) sample after annealing, (b) sample heated up 800℃ in Argon and (c) sample heated up to 1200℃ in Argon

The intrinsic features make nanoparticles tend to aggregate and it is difficult to disperse nanoparticles well in ethanol. So compared to individual micro-particles covered by coating, nanoparticles would tend to form an aggregation first and then it would be covered by coating. The passivation layer of Al_2O_3 still exist as the barrier between Al and CuO. During the annealing process, small spherical particles would be attached on the surface of Al core particles again.

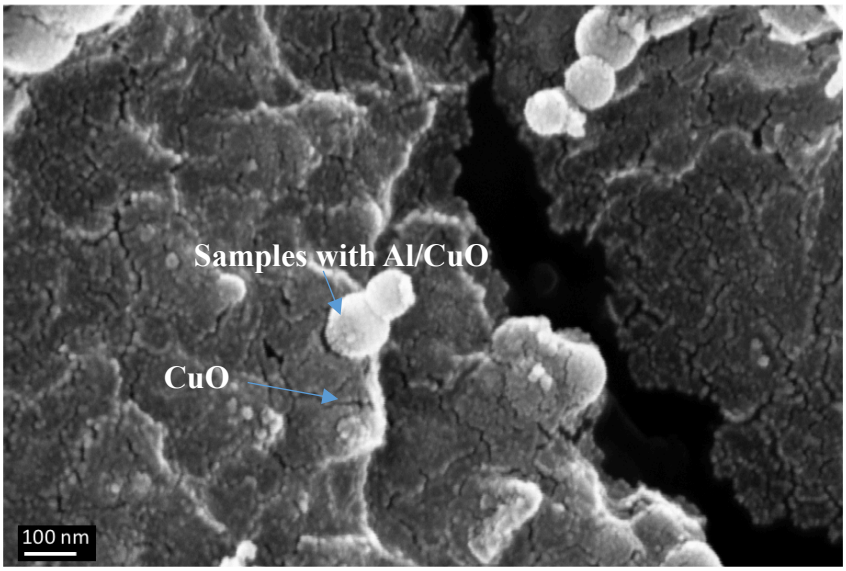

Figure3. 9 SEM image of Al/CuO nano-sized sample with equivalence ratio of 1

From SEM, we could barely see those agglomerates of CuO like what we see in the Al/CuO microparticles. But they are also present with small particles in Al/CuO nanoparticles as shown in Fig3.8. From Fig.3.9 (a), as-purchased Al nanoparticles with average diameter of 40 nm were measured with TEM and the amorphous passivation layer could be observed from that. The core spherical particle has a diameter of about 100 nm if the passivation layer is not taken into account and the thickness of the amorphous layer was measured with scale bar, which is about 8nm. As shown in Fig. 3.9 (b), the assembled Al/CuO nanoparticles tend to form clusters, similarly to SEM result in Fig. 3.8. There are also clusters of CuO with irregular shapes attached to the surface of spherical Al particles. The controversial point of the nano-structure is if Al nanoparticles are covered by a layer of CuO on the surface, which is same as the successfully coated sample in the Al/CuO microparticles. Due to continuous shifting, we could not perform EDS mapping on the nanoparticles and the exact location of different elements still need more proof. While the thickness of outer layer of Al particles with a diameter of about 100 nm in Fig.

3.9 (b) is about 15 nm exceeding 8 nm in as purchased Al nanoparticles. The difference in thickness could be caused by Al nanoparticle intrinsic variations or a successful coating. The EDS result performed during SEM measurement is shown as below in Fig. 3.10, the spherical particles attached together and the EDS result showed a high atomic percentage of the Cu element, and that could not all come from the irregular attachments on the surface. So it is possible for Al/CuO nanoparticles that both coating morphologies exist as well, but the nanoparticles are not coated individually. They form small clusters and then they are covered by CuO layer with CuO clusters at the same time.

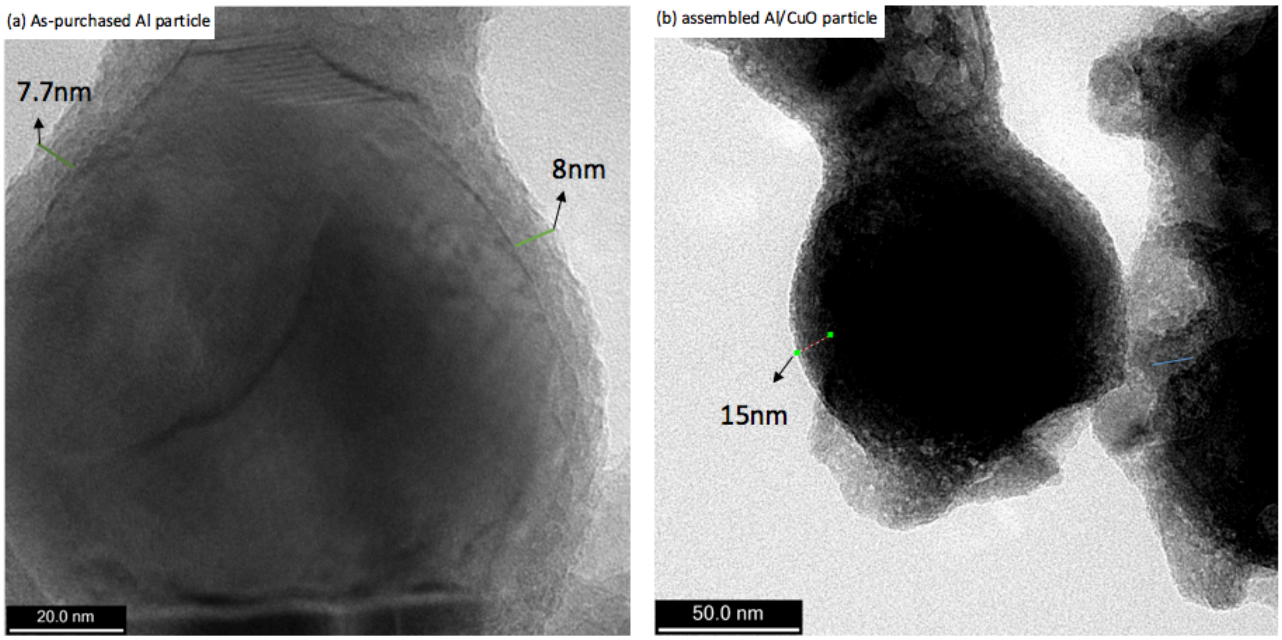

Figure3. 10 TEM images of: (a) as-purchased Al nanoparticles with average diameter of 40 nm; (b) assembled Al/CuO sample

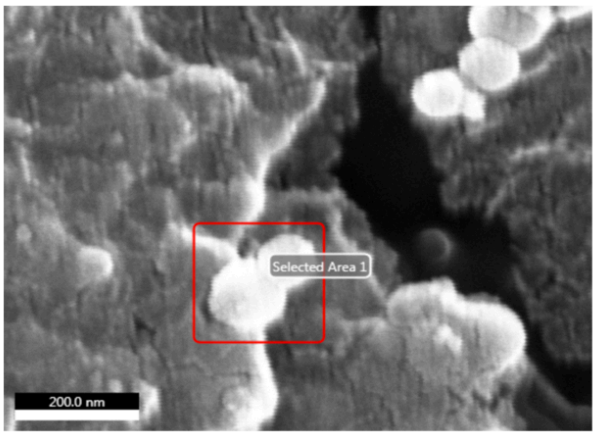

Element	Weight %	Atomic %
O K	14.13	31.65
AlK	26.01	34.57
CuK	59.86	33.78

Figure3. 11 EDS of the assembled Al/CuO sample at the same location of the SEM image

4.0 Results and discussion

4.1 Thermochemical properties of samples under low heating rates

4.1.1 DSC and TGA results of Al/CuO microparticles

Samples 1, 2 and 3, which have the equivalence ratio of 5, 3 and 1 respectively, are tested in DSC and the results are shown in Fig. 4.1. The reaction properties of these DSC curves are summarized in Table 2. Regarding the mass change, Sample 1 exhibits the smallest mass decrease, while Sample 3 shows the greatest mass change. Note that Sample 1 contains the least content of CuO, due to its large equivalence ratio. It is believed that less moisture is stored in the porous CuO shell of Sample 1, and therefore when the temperature increases, mass reduction caused by the water vaporization is smaller. It is also possible that this mass reduction is caused by the decomposition of the CuO shell which releases gaseous oxygen to the environment. Since Sample3 contains more CuO compared to the other two samples, its mass reduction is greatest among these samples.

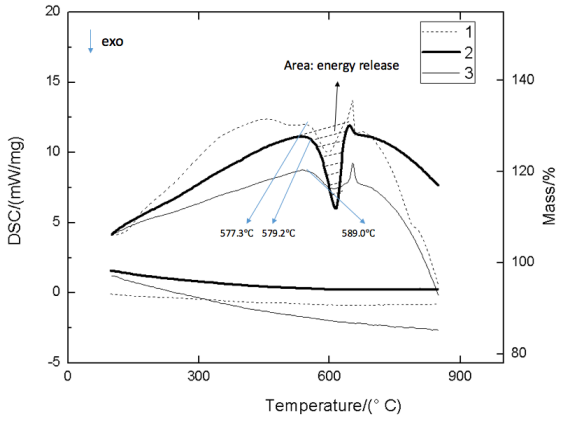

Figure4. 1 DSC and TGA (mass) results of the three samples with different equivalence ratios: (1) 5, (2) 3 and (3) 1, respectively.

Table 4- 1 The thermochemical properties of samples with core-shell structure

sample	Equivalent ratio	Onset Temperature (℃)	Energy release (J/g)
1	5	577.3	551
2	3	579.2	807
3	1	589	672

As shown in table 4-1, the three samples possess a main exothermic peak before the melting peak of Al. The melting peak of Aluminum illustrates that the shell of CuO contains less amount than the amount required to oxidize all the Al core. The onset temperature increases slightly with higher equivalence ratio, since lower equivalence ratio represents more amount of CuO. And more oxygen from CuO would be diffused to Al when the reaction was initiated, so the onset temperature of sample with more CuO would be lower. Sample 2 with an equivalence ratio of 3 would have the highest energy release, 0.8kJ/g for the main exothermic reaction indicating that the thickness of the shell of CuO would be the largest. The lower exothermic energy compared to the theoretical value comes from that some of Al particles was not successfully coated with the CuO shell as shown in figure4. The larger concentration of $[Cu(NH4)]^{2+}$ ion in solution causes agglomeration, preventing thicker shell around the Al particles. For example, the sample3 with equivalence ratio of 1 would have a relatively smaller amount of energy release. Also, there would be a smaller melting peak of Al of sample3 compared to that of sample1 with an equivalence ratio of 5. In DSC result of sample3, a weak exothermic peak at about 830℃, when liquid aluminum might diffuse through the shell to react with the CuO agglomerates. A large amount of energy required for rest Al particles to pass through the shell and this could lead to a small exothermic peak. For thermite

reactions applied in micro systems, larger amount of energy release and lower onset temperature would be preferred, so the sample 1 with an equivalence ratio of 3 would be more suitable for applications. The DSC data of the sample 1 with an equivalence ratio of 5 would have the largest melting peak of Al. Meanwhile, the sharper exothermic peak represents better combination between the CuO shell and the Al core. The decrease in mass detected by TGA was caused by the decomposition of CuO to release gas-phase oxygen to the environment. Since sample3 contain more CuO compared to the other two samples, the decrease in mass would be larger than others as well.

Table 4- 2 Sample properties and the derived activation energy data for the core-shell micro-particles in this study, the reference sample and the literature Al oxidation in oxygen

		Sample with the core-shell structure	Reference sample of micro Al and nano CuO	$Al+O_2$[61]
Particle sizes:	Al	1 μm	1 μm	1 μm
	CuO	Various layer thickness	40 *nm*	
Onset temperature (℃)		580	595	585
Energy release (J/g)		807	450	11200
Activation energy of main exothermic peak (kJ/mol)		328	438	160

The heat release characteristics of samples were further investigated under different heating rates. Different ignition methods with different heating rates would affect the performance of the thermite, and meanwhile the reaction mechanism of thermite reaction would be influenced by the

heating rate.[62] As shown in Fig. 4.2 (a), the heat release peak became broader when the heating rate was increased, because larger spatial heterogeneity for the sample with higher heating rates.[44] Moreover, the onset temperatures increased significantly with higher heating rates, which is a typical characteristic of thermal lag. Pantoya and Granier have reported similar characteristics for Al/MoO_3 NP thermites.[17] The global activation energy could be expressed as

$$\ln\left(\frac{\beta_i}{T_{Pi}^2}\right) = \ln\left(\frac{ZR}{E_a}\right) - \frac{E_a}{RT_{Pi}} \quad \text{(Eq. 4-1)}$$

where R is the gas constant (8.314 J/mol K), β is the heating rate (K/min), T_p is the temperature of the exothermic peak, Z is pre-exponential factor and E_a stands for the activation energy. The value of the activation energy E_a can be calculated from the slope of $\ln\left(\frac{\beta_i}{T_{Pi}^2}\right)$, as shown in Fig. 4.2(b). The derived activation energies are listed in Table 4-2. The core-shell structure with the equivalence ratio of 3 possesses the activation energy of 328 kJ/mol, while the reference sample with the same equivalence ratio has the activation energy of 438 kJ/mol. This reduced activation energy indicates the thermite reaction of these core-shell microparticles can be ignited at a lower onset temperature. Note that, due to the existence of the passivation Al_2O_3 layer between the Al core and the CuO shell, oxygen has to diffuse through the Al_2O_3 layer before the thermite reaction is initiated. When the heat and mass transfer paths are shortened to a negligible degree, the reaction mechanism of the core-shell structure becomes more similar to the reaction between Al micro-particles and gaseous oxygen. While the CuO layer partially covers the Al core, so the growth of Al_2O_3 amorphous layer is limited so the diffusion distance would be shorter than that of the reaction between Al and O_2. The shorter diffusion distance decreases the activation energy of the thermite reaction.

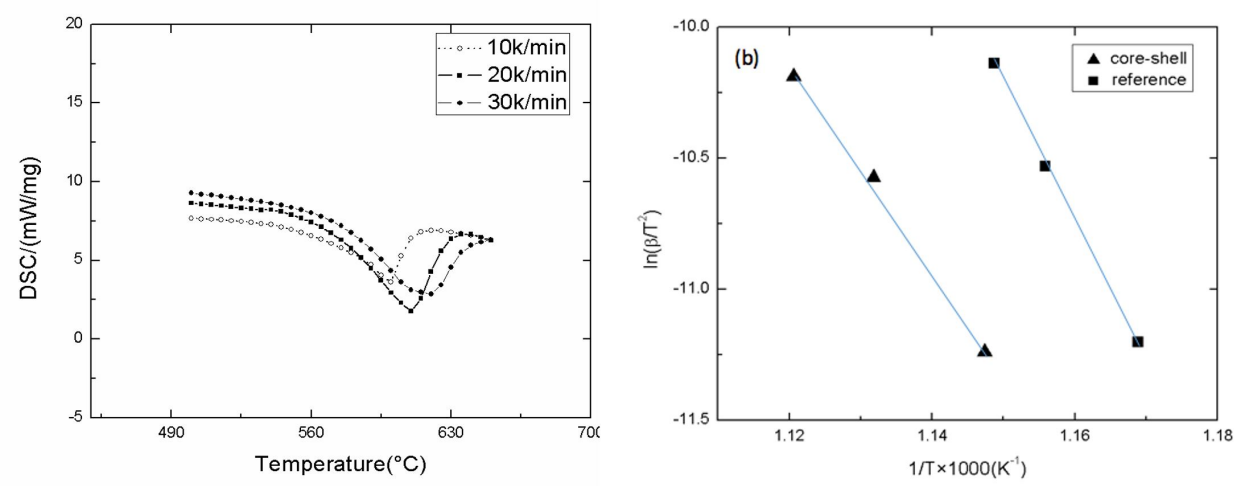

Figure4. 2 DSC traces for reactions of CuO/Al core-shell particles with heating rates of 10 K/min(1), 20K/min(2) and 30K/min(3) (b) Analysis of DSC traces

4.1.2 DSC and TGA results of Al/CuO nanoparticles

There are three sample prepared of Al/CuO nanoparticles with equivalence ratio of 1, 2 and 3. They are measured under argon as well and the heating rate for these three samples are 20K/min. The DSC results of these samples are shown as below in table and figure. Sample 1 with equivalence ratio of 1 possesses the lowest onset temperature of first exothermic peak at 561.7℃, which is similar to that of Al/CuO microparticles. The energy release of sample 1 is much larger than that of the other two samples since there is no second exothermic peak for sample1. As illustrated in table, both sample 2 and sample3 have second exothermic peaks and the onset temperature of second exothermic peak for sample2 is 83.7℃ lower than that for sample3. According to this difference, we could speculate that the onset temperature of second exothermic peak for sample1 were about 670℃. The first exothermic reaction has not fully completed at that

temperature, so two peaks are combined as one large exothermic peak. Meanwhile, sample1 has the largest melting peak of Cu, corresponding to XRD result(c) which contains a strong peak for Cu as well. For sample2 with equivalence ratio of 2, the onset temperature of two exothermic peaks are 576℃ and 762.2 ℃ respectively. It is a fuel-rich sample but there is no melting peak for Al. It is possible that the amount of Al is small and the energy required for melting Al is compensated by the huge amount of energy release since the melting temperature of Al, about 660℃ located right in the middle of two exothermic reactions. Similarly, it has a smaller melting peak for Cu around 1100℃. For sample3 with equivalence ratio of 3, two areas of energy release are better defined since the onset temperature of second exothermic peak is increased much more than that of the first one. Moreover, there is a small melting peak for Al since ER of 3 makes the amount of Al far more than CuO in this sample. There is no melting peak for Cu at around 1100℃, and it is possible that the formation of spinel Al_2CuO_4 took the major part of Cu.

Table 4- 3 The thermal characteristics of sample1, 2 and 3 of Al/CuO nanoparticles

Sample No.	Equivalence ratio	Onset temperature of first exothermic peak (℃)	Energy release of first exothermic peak(J/g)	Onset temperature of second exothermic peak(℃)
1	1	561.7	1832	/
2	2	576.6	1245	762.2
3	3	587.9	970.8	845.9

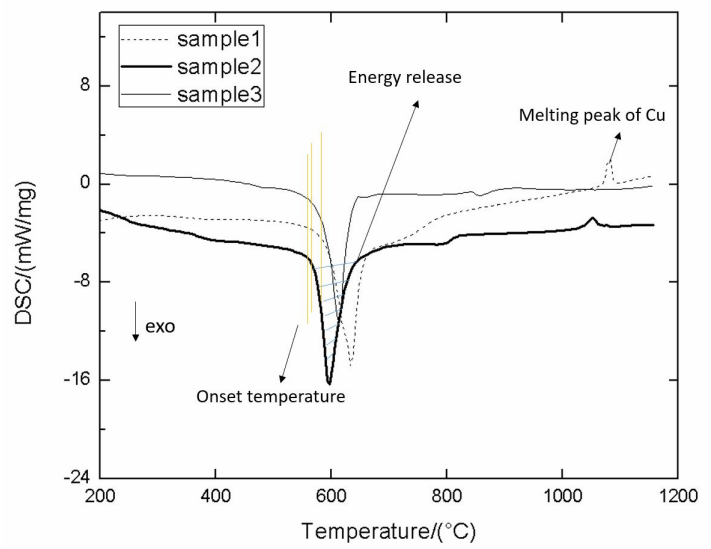

Figure4. 3 DSC results of *sample1, sample2, and sample3 with equivalence ratios of 1, 2 and 3 respectively*

TGA results of sample1, sample2, and sample3 with equivalence ratios of 1, 2 and 3 respectively are shown in Fig. 4.4. There is relatively larger decrease in mass for nano-particles compared to that of micro-particles and the mass drop increases with higher equivalence ratio. There are two possible reasons for that: 1) some copper complex formed during the synthesis procedures which released NO_2 during heating; 2) the decomposition of CuO to the environment.

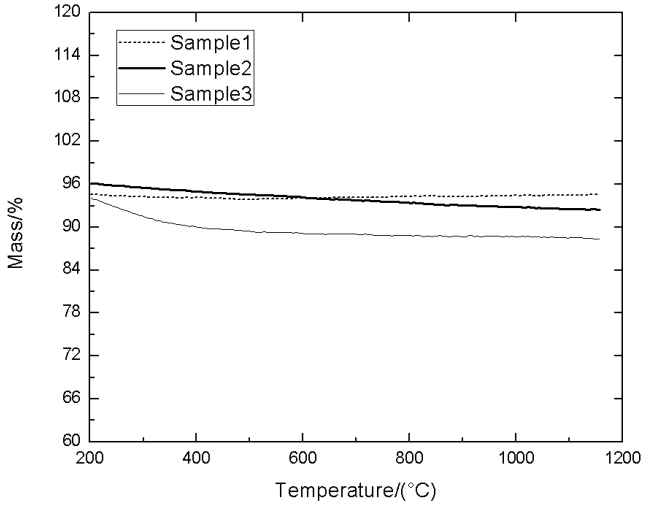

Figure4. 4 TGA results of sample1, sample2, and sample3 with equivalence ratios of 1, 2 and 3 respectively

4.2 Effects of equivalence ratio on laser ignition of core-shell Al/CuO particles

4.2.1 Introduction

As mentioned previously, the increasing interest in thermites research is related to their potential application in nano-joining, micro-propulsion, and MEMs systems. Ammunition primers which could be ignited by low-power laser would be one of possible application for nanothermites as well since traditional lead primers are harmful to user and the environment.[63] Integrated with MEMs systems, a lot of research for application as pressure-driven membrane actuators, initiators and spot heaters has been completed. New development direction for nano- and micro- thermites has been introduced to the biological area such as antimicrobial energetic systems.

For MEMs system, device components are built up with a limited size and high sensitivity which requires a precise control on the ignition of thermites. Pyrotechnic approaches have been the most widely used method for ignition of thermites since the heat transfer is promising and straightforward.[64,65] With the development of microfabrication technology, the micro-heaters have been successfully assembled on a chip while the expensive cost, high voltage requirement and high power consumption plague the spread of nano- and micro- thermites in portable devices.[26] The controllable laser power density and various spot sizes through focusing lens enable them to provide a precise amount of energy to specific locations in most devices, which possess the ability to focus on the thermites without heating up the whole devices. Fragile components could avoid the threat of deformation and distortion during the heating process.

Usually, bulky equipment and the high-power source are required to trigger laser beams onto nano- and micro- energetic materials and previously Nam-su et al were able to produce low-cost polymeric lens to further decrease the power source required for laser to about 500 mW.[26] The polymeric lens could be easily produced by putting polydimethylsiloxane into a glass based mold in a reproducible manner. With this technique, more micro- and nano- thermites could be introduced into portable and disposable devices with a more convenient ignition method.

The advantages of laser ignition and possible improvement on laser ignition have been addressed as above, so this study focus the characteristics of micro- and nano- thermites with different equivalent ratios under fast heating rates and samples could perform differently compared to low heating rates in DSC measurements. The reaction mechanisms leading to this difference would also be discussed.

4.2.2 Experimental

The sample used for laser ignition were prepared as methods discussion previously and the sample mass is about 3.5 mg and 1.75 mg for microparticles and nanoparticles respectively. They are held in the pellet without press, so they are in loose condition. There are 3 samples for each equivalent ratio to reduce the experimental error. All the results shown below are average value concluded from these three samples.

The experimental setup used in laser ignition and high-speed imaging is shown as Fig. 4.5. A diode laser (3.5W) with 100 ms pulse duration is utilized to ignite the pellet sample, together with a focusing lens to increase the power density of the laser from 225 W/cm^2 to 40 kW/ cm^2. The pellet would be put on a holder and the sample would be heated up from top. A photodiode with 1 ns response time will send the signal to trigger a Phantom high-speed camera to record at 200,000 fps and 500 ns exposure time with extreme dynamic range (EDR). To achieve high time resolution signals, two oscilloscopes are used.

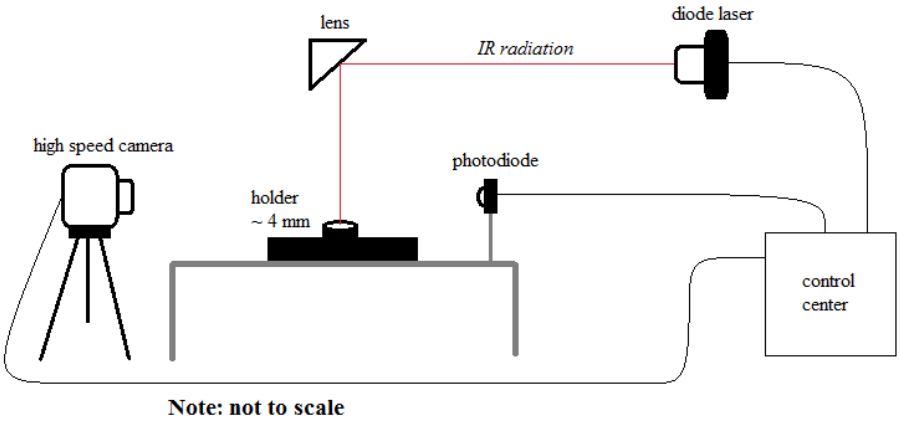

Figure4. 5 Schematic of laser ignition setup

The ignition delay could be measured from the difference of the photodiode signals of illumination and that of ignition. The first “jump” in the photodiode signal implies the starting of the laser illumination and the second one indicates the starting of the thermite reaction, which are shown in Fig. 4.6. There is a linear portion between the point of laser illumination and that of thermite reaction initiation on the curve, which indicates the ignition delay. And the time gap between the moment that laser hits the sample and the moment that the sample become more bright in high speed camera videos is also the ignition delay. They two could verify each other and all the results showed the values were comparable from these two pathways.

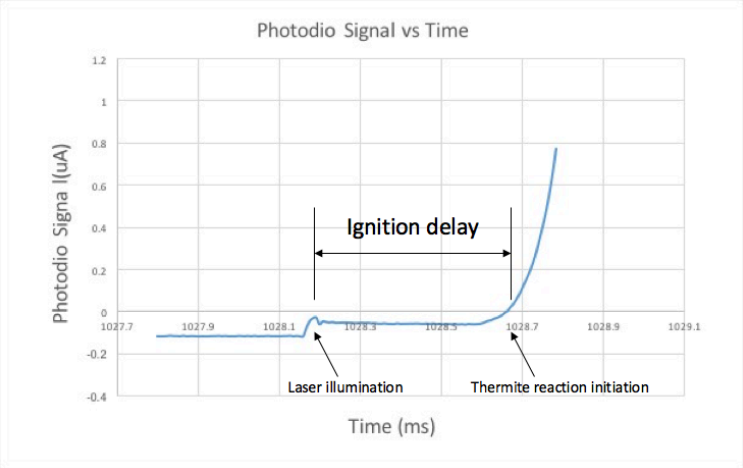

Figure4. 6 Determination of the ignition delay of the thermite reaction from photodiode signals for sample 4

The average energy release rate of the samples could also be calculated through the photodiode signal results, where the photodiode signal was integrated and normalized by the mass with respect to time.

To have a better visualization of the propagation of the burning flame and the center of the sample is assigned as position with (0, 0) when t=0 for a 2D measurement. Data of four points of the flame front would be collected and the average burning rate could be calculated

through this, which is shown in Fig. 4.7.

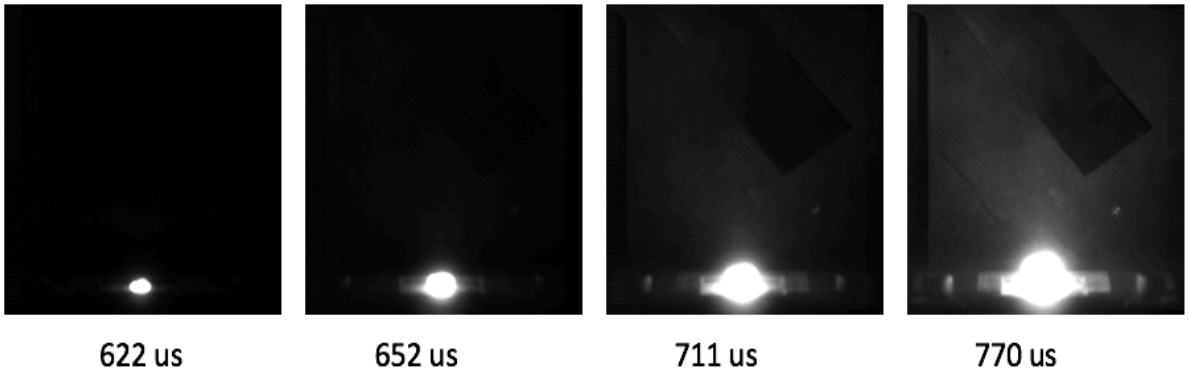

Figure4. 7 Determination of burning rate

4.2.3 Results and discussion

The ignition delays for different samples were calculated and shown in the table below. Since the results are quite different for microparticles and nanoparticles, they should be discussed respectively. As shown in table 4-4, the ignition delay increases with the increase in equivalent ratio for microparticles, while the ignition delay is shortest for the nanoparticle sample with equivalent ratio of 2. Moreover, the performance of these samples has different tendency in laser ignition measurement compared to that in DSC measurement, which indicates the thermites could perform quite differently under different heating rates. The ignition delays for microparticles with equivalence ratio of 1, 3, 5 are 5.832ms, 7. 209ms and 9.065ms and that for nanoparticles with equivalence ratio of 1, 2, 3 are 0.542ms, 0.325ms, and 1.847ms. The ignition delays for nano-samples are about one magnitude lower than that for micro-samples, which indicates the smaller diffusion distance plays an important role during initiation stage.

Table4- 4 The ignition delay of samples with different equivalence ratios

	Microparticles			Nanoparticles		
Sample No.	1	2	3	4	5	6
Equivalence ratio	1	3	5	1	2	3
Ignition delay (ms)	5.832	7.209	9.065	0.542	0.325	1.847
Average burning rate (m/s)	182.70	118.36	/	31.44	27.87	3.66

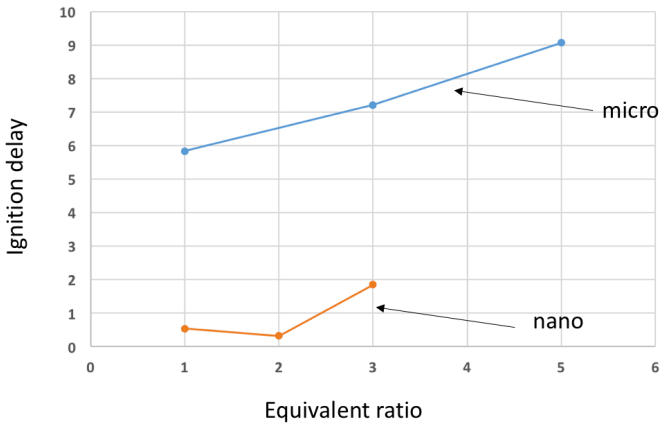

Figure4. 8 Ignition delay of samples with different equivalent ratio

As shown below, the propagation speed after initiation for micro-samples is much higher than that for nano-samples. Though microparticles have longer ignition delay, they have much larger burning rate. The expansion of flame much faster for microparticles, as shown in Fig. 4.9. Moreover, the shape of expansion of flame is different. For microparticles, the flame is spherical and very bright as shown in Fig. 4.9, while the flame is straighter and there are a lot of small

particles blown away for nanoparticles in Fig. 4.10. The average burning rates of microparticles is about 5 times than that of nanoparticles, which implies the reaction mechanism could be different for them, which will be further discussed later.

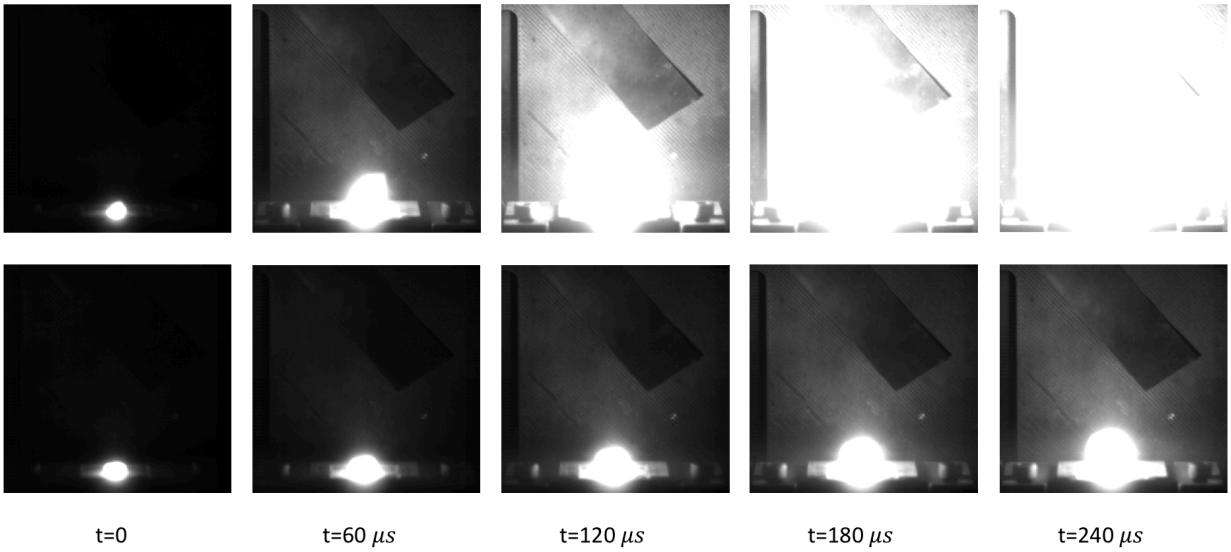

Figure4. 9 Comparison of flame expansion at the same time scale between micro-sample and nano-sample

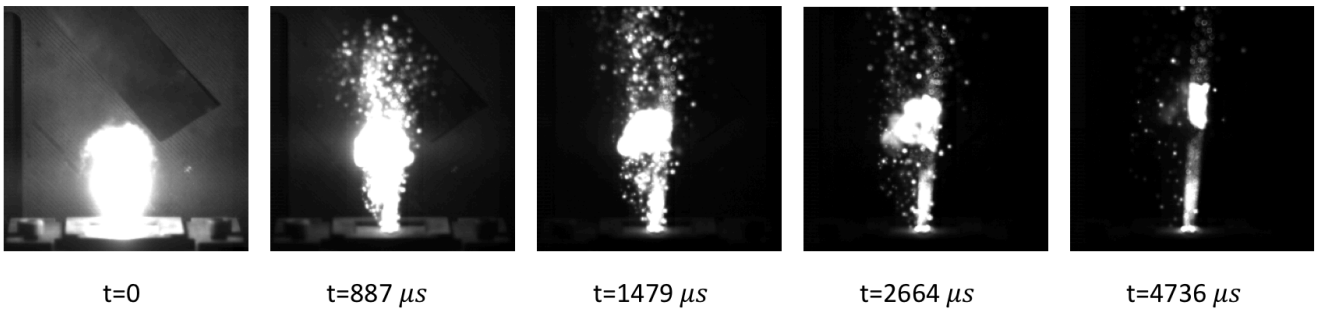

Figure4. 10 The flame propagation feature of nano-sample with equivalence ratio of 1

4.2.4 Summary

Al/CuO samples with micro-scale and nano-scale show opposite characteristics under laser ignition, since micro-samples have longer ignition delay and faster flame propagation, while nano-samples for have shorter ignition delay and slower flame propagation. For micro-samples, the ignition delay would increase with increasing equivalence ratio and the sample with equivalence ratio of 5 could not perform a self-sustain reaction. For nano-samples, the ignition delay is shortest for sample with equivalence ratio of 2 and burning rates would decrease with increasing equivalence ratio. A lot of particles have been blown away during burning, which indicates the gas production and makes the distance between particles longer for thermal conduction. The burning rate of sample with equivalence ratio of 3 is only about 3.66 m/s, which implies the large amount of gas production will hinder the thermal conduction and mass convection.

4.3Determination of reaction mechanism of Al/CuO core-shell structures

4.3.1 Introduction

To have a better understanding of the impact of structural properties on the reaction characteristics and to modify the product according to different requirements, it is vital to understand the reaction mechanism of Al/CuO particles.

Generally, most researchers think that the thermite reactions with micro-scale and nano-scale are mostly dominated by condensed phase reaction and actually they have different definition for condensed phase reaction.[66-71] Except their different conclusions, the reaction mechanism from literature could be divided into three types including condensed phase reaction, gas-surface reaction and heterogeneous reaction as shown in Fig. 4.11. For condensed phase mechanism, reactions happen between solid/solid, or solid/liquid, during which ions are transported across the interface to initiate the reaction. While for melt dispersion mechanism, Al core melt first and the pressure change caused by melting leads to spallation of the oxide shell, following by dispersion of liquid Al clusters.[72] Some researchers proposed another gas-surface mechanism, in which two major exothermic reactions were taken into account: 1)the reaction between gaseous Al after evaporation and oxidizing species such as O and AlO; 2) the reaction between melt Al and gaseous oxidizer when Al diffuses through the oxide to reach the surface.[67] The similarity between melt dispersion mechanism and gas-surface mechanism is that Al has to melt first. While the difference comes from if the oxide shell could still maintain their shape at that moment. Whereas, for heterogeneous reactions, gaseous oxygen released by CuO would pass through the oxide shell and react with core Al. For condensed phase reaction, gas-surface reaction and heterogeneous reaction,

the rate control step is the diffusion through oxide layer but with different species. The heating rate also plays an important role in determining the reaction mechanism since they could have different reaction mechanism under different heating rates.

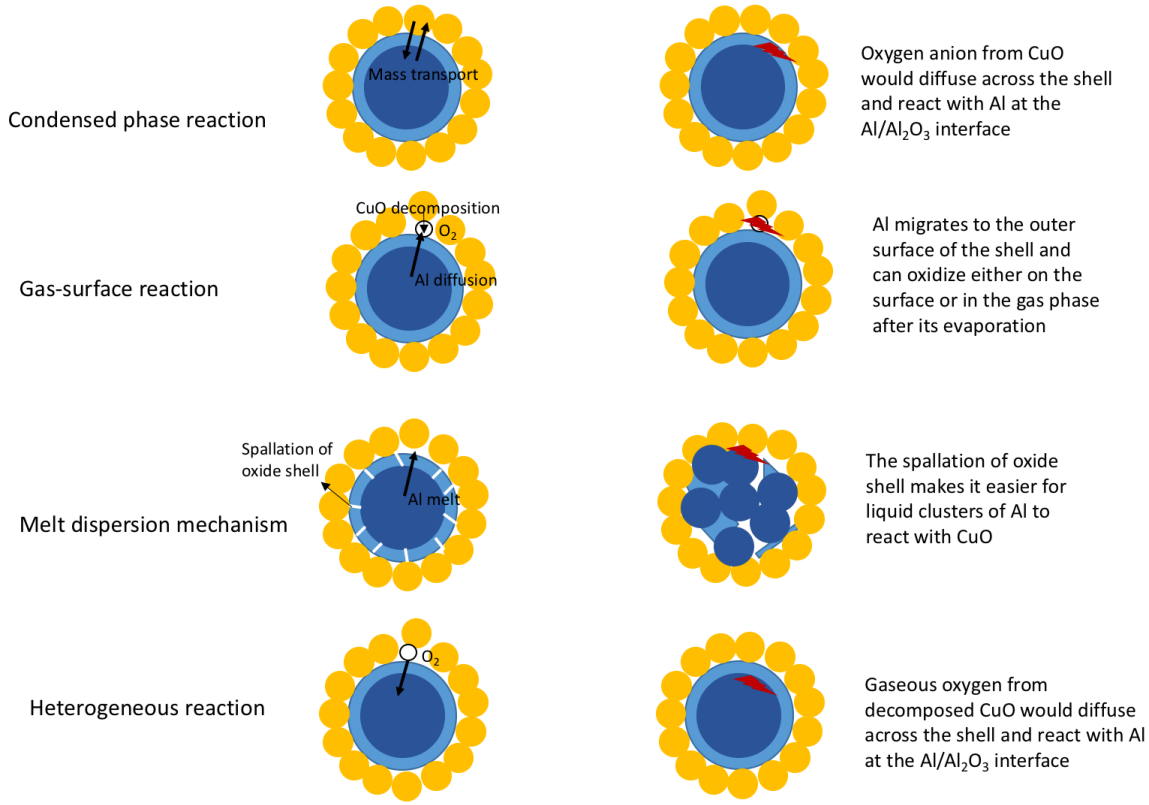

Figure4. 11 Reaction mechanisms proposed for Al/CuO system

Previously, Garth et al offered a detailed insight into the multi-frame imaging with nanometer spatial and nanosecond temporal resolution with a movie mode dynamic transmission electron microscopy (MM-DTEM) and demonstrated that CuO would first melting and then coalescence under high heating rates like laser ignition.[71] Under EDS and DTEM, none results containing any evidence for spallation of metal fuel was observed, which could be considered as the evidence of the melt dispersion mechanism.[71] Moreover, the images from DTEM proved that the loss of nano-

structure in thermite reaction under high heating rates is much faster than the occurrence of heterogeneous reaction, emphasizing the dominance of condensed phase reaction.[73] Recently, a study by Sarah *et al.* proposed a condensed phase model focus on the initiation and early stage of Al/CuO and the experimental results match the modeling results leading to a conclusion that the initiation of Al/CuO nanoparticles is governed by the condensed phase mechanism at moderate heating rates (~10^5K s^{-1}).[67] It has been proposed by Rohit et al that three different types nanothermites (Al/CuO, Al/WO_3, Al/Bi_2O_3) form similar products after combustion and quenching, which contains 90% super-microns by weight and they concluded that the reaction is controlled by condensed phase through scaling.[66] This conclusion was later modified by themselves and they implied this conclusion works for Al/WO_3, Al/Bi_2O_3 expect Al/CuO. They ignited the thermite at about 10^5K s^{-1} with a platinum wire and the product was captured and quenched rapidly with 500 μs to maintain the chemical characteristics for analysis. According to EDS result, the oxygen content in product of Al/CuO is always less than that of the other two thermites since the ignition temperature of Al/CuO nanothermites is similar to the oxygen release temperature of Al/CuO thermites.[66] So the reaction between Al and gaseous oxygen could be observed after 1ms during ignition at heating rate of 10^5K s^{-1}.

4.3.2 Discussion on the reaction mechanism of the Al/CuO micro-particles

The onset temperature of Al/CuO micro-particles with the core-shell structure is about 580℃, which would be lower than the melting temperature of Al micro-powders, similar with mixed Al/CuO nanothermites.[44,33] The exothermic reaction for this core-shell structure took place before the melting point of Al, and the oxygen in CuO shell would diffuse through the aluminum oxide

shell of aluminum particles.[74,75] The short diffusion distance and the large contact area of the core-shell thermites improve the heat transfer in thermites and the reaction kinetics would be assisted.[70]

For condensed-phase reaction, the performance of the thermite would be dominant by the combination state and reactivity of metal (fuel) and the combination state of metal oxide (oxidizer).[76] For highly compacted structures like this, substitutional diffusion would be dominant in the exothermic reaction.[77,78] As illustrated in Fig. 4.12, some particles maintained spherical structure after DSC measurement. These successfully coated samples with fully covered CuO would not have enough CuO on the surface and the molten Al were not able to pass through the shell of Al_2O_3 and Cu. According to the atomic ratio from EDS result and the XRD result after reaction, Al would not be fully oxidized to Al_2O_3 for this particle, which verifies the assumption that some Al would be blocked in the middle and explains the relatively low energy release of micro-particles compared to nanoparticles with core-shell structures. During the initial stage of thermite reaction, oxygen ions would be accumulated at the interface of Al_2O_3 and CuO to prevent the decomposition of CuO since Al_2O_3 is one kind of inert matrix.[79] So the oxygen from CuO would diffuse through the Al_2O_3 layer and react with Al core to form thicker Al_2O_3 layer. As mentioned previously, amorphous Al_2O_3 would start to transform to γ-Al_2O_3 when begins when diffusion resistance of γ-Al_2O_3 exceeds that of the shrinking layer of the amorphous Al_2O_3 though the oxide layer incorporating of separate individual crystallite structures growing among the amorphous layer leading to a low diffusion resistance.[80] Before the thermite reaction, the environment of sample in DSC appears endothermic feature, which corresponds to the oxidative growth period of amorphous Al_2O_3.[79,80]

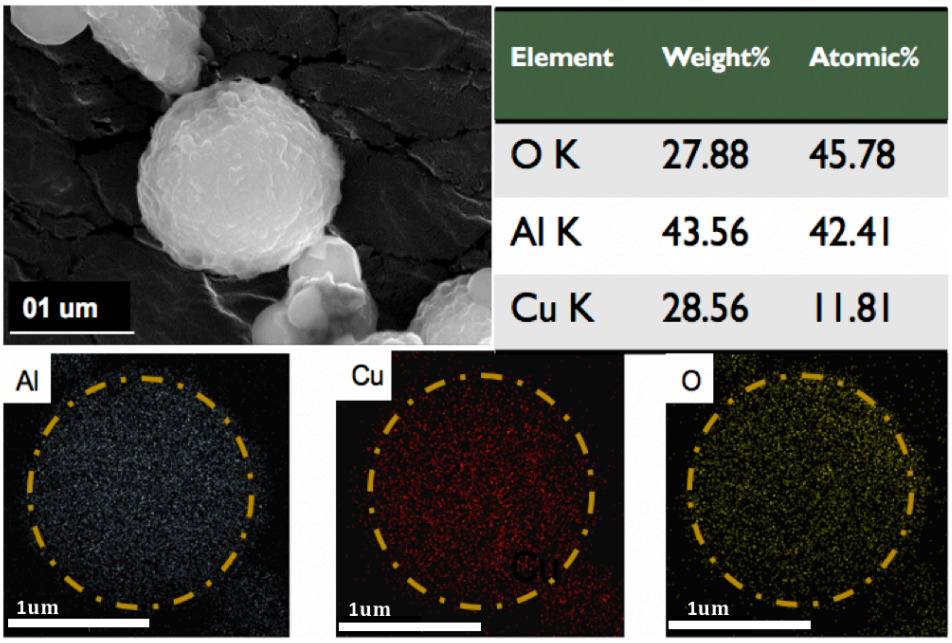

Figure4. 12 SEM image and EDS mapping of the Al/CuO particle after the reaction

5.3.3 Study of reaction mechanism of Al/CuO nano-sized particles

The Fig. 4.13 compares the flame difference of sample with ER=1 and sample with ER=3. There are a lot of particles blown away in both pictures while the shape for (a) still keeps straight and the particles are closer. For Fig. 4.13, some particles are far away from the middle, which makes a long distance for heat to transfer. In DSC measurements, the mass drop of nano-sized particles is relatively larger than that of micro-sized particles and it implies more gas generated during the thermite reaction. XRD results of nano-sized particle show that Cu_2O formed after being heated up to 800℃ and this could imply the decomposition of CuO.

So it should be dominant by heterogeneous reaction mechanism for Al/CuO nano-sized

particles with spherical core-shell structure under high heating rates such as laser iginition. And the reaction rate is limited by heterogeneous Al-O_2 reaction.

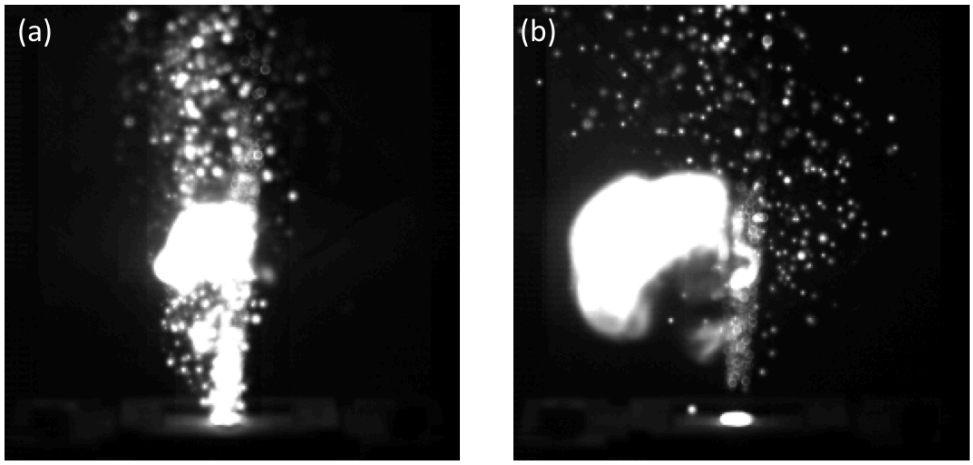

Figure4. 13 Comparison of flame of (a) sample with ER=1, (b) sample with ER=3

5.0 Summary and future work

5.1 Summary

This research developed a solution phase synthesis method for producing spherical Al/CuO particles with a core-shell structure. The relative structural and thermochemical properties are measured through different characterization methods. The reaction between copper nitrate and ammonium hydroxide is used to form a shell containing copper complex on Al particles with a passivation layer. After annealing, the copper complex in the shell is oxidized to CuO. Al particles of two different sizes are used, with diameters of 1 μm and 40 nm respectively. Due to the difference in size, the final morphologies of the samples are not the same and the Al particles of diameter 1 μm are coated individually. The results show both successfully and unsuccessfully coated particles at the same time according to the SEM and EDS analysis. In the case of the successfully coated particle, the Al particle is completely covered by a rough layer of CuO and attached to some small agglomerates of CuO. Since the 1 μm Al particle is quite large in comparison with the coated shell, there is some Al left over after the reaction according to the XRD results. Due to the particle structure, the unreacted Al was blocked in the middle of the particle and could not complete further reaction with free CuO agglomerates, which caused the particle to maintain a spherical structure after the reaction. In the case of the Al particles of diameter 40 nm, the intrinsic tendency to aggregation made it difficult for them to be individually coated, so a cluster of several particles is formed and coated with a layer of CuO according to the SEM and EDS analysis. Some clusters of CuO remain attached to the surface. Some Cu_2O formed at 800℃ and no CuO was found, which implies that the CuO was first reduced to Cu_2O and then the Cu_2O was reduced to Cu. At 1200℃, all the CuO was reduced to Cu and one new compound of Al_2CuO_4 is formed.

The endothermic and exothermic events in these samples were measured by DSC, along with TGA which measures the weight loss in the samples. The onset temperatures of the first exothermic peak among these samples are close and they are all lower than the melting temperature of Al. For the 1 μm Al samples, the second exothermic peak does not normally occur, or if it occurs, the energy release of the second exothermic peak is really small. This could be due to the fact that the shell becomes thicker during the thermite reaction, and this prevents the Al in the core area from flowing outside and reacting with CuO. The fuel rich sample showed the largest energy release for the first exothermic peak. The 40 nm Al samples showed an increased energy release in comparison with the 1 μm Al samples, and there is a second exothermic peak for the samples with an equivalence ratio of 2 and 3. In the case of the samples with an equivalence ratio of 1, the second exothermic peak overlapped the first exothermic peak and a larger exothermic peak was formed. Only the samples with an equivalence ratio of 3 reached the melting point of Al. The thermochemical properties of these samples were also studied under laser ignition and these showed different performances at high heating rates. The 1 μm sample with an equivalence ratio of 5 could not have a self-sustaining reaction. All the other samples underwent a self-sustaining reaction. Generally, the 1 μm Al samples show a longer ignition delay and faster flame propagation, while the 40 nm samples have a shorter ignition delay and slower flame propagation.

Based on the performance under low and high heating rates, the reaction mechanisms for spherical Al/CuO particles with a core-shell structure can be determined. The thermite reaction of the 1 μm Al samples occurs before the melting point of Al and the spherical structure is maintained after the thermite reaction in DSC measurement. Under laser ignition, the flame is bright and compressed, and no particles are visible around the flame. Hence the condensed phase

reaction is considered to be the dominant mechanism for this sample. The mass drop in TGA is slightly higher for the 40 nm samples. During laser ignition, it is clearly that a lot of particles are blown away which makes it is difficult for flame to propagate. It is difficult to determine the reaction mechanism for this particle size.

5.2 Contributions

The major contribution of this thesis is the relatively new method for the synthesis of spherical Al/CuO particles with a core-shell structure. There are several methods described in literature for Al/CuO nanowires with a core-shell structure and these do not refer to a free standing material. The requirement for a substrate makes it difficult for these methods to be applied in a flowing system and for moulding to a specific shape. For example, the proposed low-power focused-laser-assisted remote igniter still uses an Al/CuO/ethanol mixture as the energetic material to fill the hole in the polymer lens and the ethanol is later evaporated. To achieve a specific shape, the combination of a mould and a solution phase material is simple and cost-efficient. Moreover, the spherical Al/CuO micro-particle with a core-shell structure performs similarly to nanothermites in DSC measurement, so this provides an alternative to nanothermites with similar properties. This method has a shorter ignition delay in comparison with other micro-particle mixtures of Al/CuO thermite. In the case of the spherical Al/CuO nano-particle with a core-shell structure, the energy release is increased though the active content of nanoparticles is much lower than that of microparticles.

The thermochemical properties under laser ignition are important since laser ignition can be easily integrated with MEMs. Most of the samples can have a self-sustaining reaction once they are ignited by laser and this could prevent the laser from heating the whole MEMs up. The two different sizes of sample have significantly different features under laser ignition, so these

could meet different requirements.

5.3 Future work

The investigation of additional factors that could influence the thermochemical properties under laser ignition could be investigated to obtain better control of the thermite. Particularly in the case of the 1 μm Al samples, the performance is more constant in DSC measurement but the responses to laser ignition show diversity. The inclusion of more test factors could provide a better understanding of how other factors could influence the thermochemical properties under laser ignition.

In the case of the 40 nm samples, more TEM images could be taken before and after reaction to validate the heterogeneous reaction mechanism since several researchers consider the reaction between Al and CuO to be a condensed-phase reaction from both a theoretical and an experimental perspective. Whilst theoretical models of the reaction between Al and CuO are currently based on a mixture of powders or laminates, this may not be suitable for this structure, so it would provide a deeper understanding of the experimental results if a model based on the core-shell structure could be built.

The proposed low-power focused-laser-assisted remote igniter provides an interesting concept for the application of thermites in MEMs system since the igniter could be as simple as a laser pointer. The samples could be tested under laser with different wavelengths and powers to compare the performance, and to determine the minimum power to ignite the sample for a self-sustaining reaction. This would enable this application to be used in more portable and disposable devices.

References

(1) Chou, S.; Yang, W.; Chua, K.; Li, J.; Zhang, K. Development Of Micro Power Generators – A Review. *Applied Energy* 2011, *88*, 1-16.

(2) Walley, S.; Balzer, J.; Proud, W.; Field, J. Response Of Thermites To Dynamic High Pressure And Shear. *Proceedings of the Royal Society of London. Series A: Mathematical, Physical and Engineering Sciences* 2000, *456*, 1483-1503.

(3) S, B. *Chemistry And Physics Of Energetic Materials*; Springer Netherlands: Dordrecht, 1990.

(4) Sui, H.; Li, B.; Wen, J. Interaction Between Single-Walled Carbon Nanotubes And Reactive Nanoparticle Constituents In Multilayered Al/Nio Nanocomposite. *ACS Applied Energy Materials* 2018.

(5) Dreizin, E. Metal-Based Reactive Nanomaterials. *Progress in Energy and Combustion Science* 2009, *35*, 141-167.

(6) Wang, L.; Munir, Z.; Maximov, Y. Thermite Reactions: Their Utilization In The Synthesis And Processing Of Materials. *Journal of Materials Science* 1993, *28*, 3693-3708.

(7) Lopresti, J.; Davis, D.; Kalay, S. Strengthening The Track Structure For Heavy Axle Loads. *Railway Track & Structures* 2002, 21-26.

(8) Routh, E. *Engineering Reactivity In Thermite Reactive Nano-Laminates*; NC: North Carolina State University: Raleigh, 2018.

(9) Lafontaine, E.; Comet, M. In *Nanothermites*; ISTE Ltd, 2016.

(10) Pantoya, M.; Granier, J. Combustion Behavior Of Highly Energetic Thermites: Nano Versus Micron Composites. *Propellants, Explosives, Pyrotechnics* 2005, *30*, 53-62.

(11) Aumann, C. Oxidation Behavior Of Aluminum Nanopowders. *Journal of Vacuum Science & Technology B: Microelectronics and Nanometer Structures* 1995, *13*, 1178.

(12) Xu, D.; Yang, Y.; Cheng, H.; Li, Y.; Zhang, K. Integration Of Nano-Al With Co3o4 Nanorods To Realize High-Exothermic Core–Shell Nanoenergetic Materials On A Silicon Substrate. *Combustion and Flame* 2012, *159*, 2202-2209.

(13) Zhou, X.; Xu, D.; Zhang, Q.; Lu, J.; Zhang, K. Facile Green In Situ Synthesis Of Mg/Cuo Core/Shell Nanoenergetic Arrays With A Superior Heat-Release Property And Long-Term Storage Stability. *ACS Applied Materials & Interfaces* 2013, *5*, 7641-7646.

(14) Dreizin, E.; Schoenitz, M. Correlating Ignition Mechanisms Of Aluminum-Based Reactive Materials With Thermoanalytical Measurements. *Progress in Energy and Combustion Science* 2015, 50, 81-105.

(15) Fischer, S.; Grubelich, M. Theoretical Energy Release Of Thermites, Intermetallics, And Combustible Metals. In *The 24th International Pyrotechnics Seminar*; Monterey, 1998.

(16) Baijot, V.; Glavier, L.; Ducéré, J.; Djafari Rouhani, M.; Rossi, C.; Estève, A. Modeling The Pressure Generation In Aluminum-Based Thermites. *Propellants, Explosives, Pyrotechnics* 2015, *40*, 402-412.

(17) Pantoya, M.; Granier, J. The Effect Of Slow Heating Rates On The Reaction Mechanisms Of Nano And Micron Composite Thermite Reactions. *Journal of Thermal Analysis and Calorimetry* 2006, *85*, 37-43.

(18) Meir, Y.; Jerby, E. Underwater Microwave Ignition Of Hydrophobic Thermite Powder Enabled By The Bubble-Marble Effect. *Applied Physics Letters* 2015, *107*, 054101.

(19) Ardila Rodríguez, G.; Suhard, S.; Rossi, C.; Estève, D.; Fau, P.; Sabo-Etienne, S.; Mingotaud, A.; Mauzac, M.; Chaudret, B. A Microactuator Based On The Decomposition Of An Energetic Material For Disposable Lab-On-Chip Applications: Fabrication And Test. *Journal of*

Micromechanics and Microengineering 2008, *19*, 015006.

(20) Hacker, D.; Lieberman, P. Thermodynamic Performance Evaluation Of A Hydroduct Using A Thermite Fuel. *Journal of Hydronautics* 1969, *3*, 139-144.

(21) Apperson, S.; Bezmelnitsyn, A.; Thiruvengadathan, R.; Gangopadhyay, K.; Gangopadhyay, S.; Balas, W.; Anderson, P.; Nicolich, S. Characterization Of Nanothermite Material For Solid-Fuel Microthruster Applications. *Journal of Propulsion and Power* 2009, *25*, 1086-1091.

(22) Sullivan, K.; Wu, C.; Piekiel, N.; Gaskell, K.; Zachariah, M. Synthesis And Reactivity Of Nano-Ag2o As An Oxidizer For Energetic Systems Yielding Antimicrobial Products. *Combustion and Flame* 2013, *160*, 438-446.

(23) Korampally, M.; Apperson, S.; Staley, C.; Castorena, J.; Thiruvengadathan, R.; Gangopadhyay, K.; Mohan, R.; Ghosh, A.; Polo-Parada, L.; Gangopadhyay, S. Transient Pressure Mediated Intranuclear Delivery Of FITC-Dextran Into Chicken Cardiomyocytes By MEMS-Based Nanothermite Reaction Actuator. *Sensors and Actuators B: Chemical* 2012, *171-172*, 1292-1296.

(24) Bodsworth, C. *The Extraction And Refining Of Metals*; Routledge: Boca Raton, 2018.

(25) Wang, K.; Lin, K.; Lee, C. Melting Of Municipal Solid Waste Incinerator Fly Ash By Waste-Derived Thermite Reaction. *Journal of Hazardous Materials* 2009, 162, 338-343.

(26) Jang, N.; Ha, S.; Kim, K.; Cho, M.; Kim, S.; Kim, J. Low-Power Focused-Laser-Assisted Remote Ignition Of Nanoenergetic Materials And Application To A Disposable Membrane Actuator. *Combustion and Flame* 2017, *182*, 58-63.

(27) Umbrajkar, S.; Schoenitz, M.; Dreizin, E. Exothermic Reactions In Al–CuO Nanocomposites. *Thermochimica Acta* 2006, *451*, 34-43.

(28) Sui, H.; LeSergent, L.; Wen, J. Diversity In Addressing Reaction Mechanisms Of Nano-Thermite Composites With A Layer By Layer Structure. *Advanced Engineering Materials* 2017, *20*, 1700822.

(29) Sui, H.; Atashin, S.; Wen, J. Thermo-Chemical And Energetic Properties Of Layered Nano-Thermite Composites. *Thermochimica Acta* 2016, *642*, 17-24.

(30) Wang, H.; DeLisio, J.; Jian, G.; Zhou, W.; Zachariah, M. Electrospray Formation And Combustion Characteristics Of Iodine-Containing Al/CuO Nanothermite Microparticles. *Combustion and Flame* 2015, *162*, 2823-2829.

(31) Qin, L.; Gong, T.; Hao, H.; Wang, K.; Feng, H. Core–Shell-Structured Nanothermites Synthesized By Atomic Layer Deposition. *Journal of Nanoparticle Research* 2013, *15*.

(32) Zheng, G.; Zhang, W.; Shen, R.; Ye, J.; Qin, Z.; Chao, Y. Three-Dimensionally Ordered Macroporous Structure Enabled Nanothermite Membrane Of Mn2o3/Al. *Scientific Reports* 2016, *6*.

(33) Petrantoni, M.; Rossi, C.; Salvagnac, L.; Conédéra, V.; Estève, A.; Tenailleau, C.; Alphonse, P.; Chabal, Y. Multilayered Al/Cuo Thermite Formation By Reactive Magnetron Sputtering: Nano Versus Micro. *Journal of Applied Physics* 2010, *108*, 084323.

(34) Bahrami, M.; Taton, G.; Conédéra, V.; Salvagnac, L.; Tenailleau, C.; Alphonse, P.; Rossi, C. Magnetron Sputtered Al-Cuo Nanolaminates: Effect Of Stoichiometry And Layers Thickness On Energy Release And Burning Rate. *Propellants, Explosives, Pyrotechnics* 2014, *39*, 365-373.

(35) Kuntz, J.; Cervantes, O.; Gash, A.; Munir, Z. Tantalum–Tungsten Oxide Thermite Composites Prepared By Sol–Gel Synthesis And Spark Plasma Sintering. *Combustion and Flame* 2010, *157*, 1566-1571.

(36) Walker, J.; Tannenbaum, R. Formation of Nanostructured Energetic Materials Via Modified Sol-Gel Synthesis. *MRS Proceedings* 2003, *800*.

(37) Séverac, F.; Alphonse, P.; Estève, A.; Bancaud, A.; Rossi, C. High-Energy Al/Cuo Nanocomposites Obtained By DNA-Directed Assembly. *Advanced Functional Materials* 2011, *22*, 323-329.

(38) Hosseini, S.; Sheikhpour, A.; Keshavarz, M.; Tavangar, S. The Effect Of Metal Oxide Particle Size On The Thermal Behavior And Ignition Kinetic Of Mg–Cuo Thermite Mixture. *Thermochimica Acta* 2016, *626*, 1-8.

(39) Dutro, G.; Yetter, R.; Risha, G.; Son, S. The Effect Of Stoichiometry On The Combustion Behavior Of A Nanoscale Al/Moo3 Thermite. *Proceedings of the Combustion Institute* 2009, *32*, 1921-1928.

(40) Kwon, J.; Ducéré, J.; Alphonse, P.; Bahrami, M.; Petrantoni, M.; Veyan, J.; Tenailleau, C.; Estève, A.; Rossi, C.; Chabal, Y. Interfacial Chemistry In Al/Cuo Reactive Nanomaterial And Its Role In Exothermic Reaction. *ACS Applied Materials & Interfaces* 2013, *5*, 605-613.

(41) Zhang, T.; Wang, Z.; Li, G.; Luo, Y. Tuning The Reactivity Of Al/Fe2o3 Nanoenergetic Materials Via An Approach Combining Soft Template Self-Assembly With Sol–Gel Process Process. *Journal of Solid State Chemistry* 2015, *230*, 1-7.

(42) Cheng, J.; Hng, H.; Ng, H.; Soon, P.; Lee, Y. Synthesis And Characterization Of Self-Assembled Nanoenergetic Al–Fe2o3 Thermite System. *Journal of Physics and Chemistry of Solids* 2010, *71*, 90-94.

(43) Kim, D.; Bae, J.; Kang, M.; Kim, H. Analysis On Thermite Reactions Of Cuo Nanowires And Nanopowders Coated With Al. *Current Applied Physics* 2011, *11*, 1067-1070.

(44) Ohkura, Y.; Liu, S.; Rao, P.; Zheng, X. Synthesis And Ignition Of Energetic Cuo/Al Core/Shell Nanowires. *Proceedings of the Combustion Institute* 2011, *33*, 1909-1915.

(45) Fritz, G.; Spey, S.; Grapes, M.; Weihs, T. Thresholds For Igniting Exothermic Reactions In Al/Ni Multilayers Using Pulses Of Electrical, Mechanical, And Thermal Energy. *Journal of Applied Physics* 2013, *113*, 014901.

(46) Luman, J.; Wehrman, B.; Kuo, K.; Yetter, R.; Masoud, N.; Manning, T.; Harris, L.; Bruck, H. Development And Characterization Of High Performance Solid Propellants Containing Nano-

Sized Energetic Ingredients. *Proceedings of the Combustion Institute* 2007, *31*, 2089-2096.

(47) Seim, H.; Nieminen, M.; Niinistö, L.; Fjellvåg, H.; Johansson, L. Growth Of Lacoo3 Thin Films From B-Diketonate Precursors. *Applied Surface Science* 1997, *112*, 243-250.

(48) Yang, T.; Cho, W.; Kim, M.; An, K.; Chung, T.; Kim, C.; Kim, Y. Atomic Layer Deposition Of Nickel Oxide Films Using Ni(Dmamp)2 And Water. *Journal of Vacuum Science & Technology A: Vacuum, Surfaces, and Films* 2005, *23*, 1238-1243.

(49) Ferguson, J.; Buechler, K.; Weimer, A.; George, S. Sno2 Atomic Layer Deposition On Zro2 And Al Nanoparticles: Pathway To Enhanced Thermite Materials. *Powder Technology* 2005, *156*, 154-163.

(50) Floro, J. Propagation Of Explosive Crystallization In Thin Rh–Si Multilayer Films. *Journal of Vacuum Science & Technology A: Vacuum, Surfaces, and Films* 1986, *4*, 631-636.

(51) Coker, A.; Ludwig, E. *Ludwig's Applied Process Design For Chemical And Petrochemical Plants*; Elsevier: Amsterdam, 2010.

(52) Sullivan, K. IGNITION, COMBUSTION AND TUNING OF NANOCOMPOSITE THERMITES. Ph.D, University of Maryland, 2010.

(53) Bazyn, T.; Glumac, N.; Krier, H.; Ward. T.; Schoenitz, M.; Dreizin, E. Reflected shock ignition and combustion of aluminum and nanocomposite thermite powders. *Combustion Science and Technology* 2007, 179, 457-476.

(54) Dimitriou, P.; Hlavacek, V.; Valone, S.; Behrens, R.; Hansen, G.; Margrave, J. Laser-Induced Ignition In Solid-State Combustion. *AIChE Journal* 1989, *35*, 1085-1096.

(55) SON, S.; QUINN BREWSTER, M. RADIATION-AUGMENTED COMBUSTION OF HOMOGENEOUS SOLIDS. *Combustion Science and Technology* 1995, *107*, 127-154.

(56) Sanders, V.; Asay, B.; Foley, T.; Tappan, B.; Pacheco, A.; Son, S. Reaction Propagation Of

Four Nanoscale Energetic Composites (Al/Moo3, Al/WO3, Al/Cuo, And B12O3). *Journal of Propulsion and Power* 2007, *23*, 707-714.

(57) Jeurgens, L.; Sloof, W.; Tichelaar, F.; Mittemeijer, E. Growth Kinetics And Mechanisms Of Aluminum-Oxide Films Formed By Thermal Oxidation Of Aluminum. Journal of Applied Physics 2002, 92, 1649-1656.

(58) Jeurgens, L.; Sloof, W.; Tichelaar, F.; Mittemeijer, E. Thermodynamic Stability Of Amorphous Oxide Films On Metals: Application To Aluminum Oxide Films On Aluminum Substrates. Physical Review B 2000, 62, 4707-4719.

(59) Egan, G.; LaGrange, T.; Zachariah, M. Time-Resolved Nanosecond Imaging Of Nanoscale Condensed Phase Reaction. *The Journal of Physical Chemistry C* 2015, 150127145402000.

(60) Lahiner, G.; Nicollet, A.; Zapata, J.; Marín, L.; Richard, N.; Rouhani, M.; Rossi, C.; Estève, A. A Diffusion–Reaction Scheme For Modeling Ignition And Self-Propagating Reactions In Al/Cuo Multilayered Thin Films. *Journal of Applied Physics* 2017, 122, 155105.

(61) Saceleanu, F.; Atashin, S.; Wen, J. Investigation Of The Effects Of Phase Transformations In Micro And Nano Aluminum Powders On Kinetics Of Oxidation Using Thermogravimetric Analysis. Physical Chemistry Chemical Physics 2017, 19, 18996-19009.

(62) Kissinger, H. Reaction Kinetics In Differential Thermal Analysis. *Analytical Chemistry* 1957, 29, 1702-1706.

(63) Petre, C.; Chamberland, D.; Ringuette, T.; Ringuette, S.; Paradis, S.; Stowe, R. LOW-POWER LASER IGNITION OF ALUMINUM/METAL OXIDE NANOTHERMITES. *International Journal of Energetic Materials and Chemical Propulsion* 2014, *13*, 479-494.

(64) Ahn, J.; Kim, S.; Kim, J.; Jang, N.; Kim, D.; Lee, H.; Kim, J.; Kim, S. A Micro-Chip Initiator With Controlled Combustion Reactivity Realized By Integrating Al/Cuo Nanothermite Composites On A Microhotplate Platform. *Journal of Micromechanics and Microengineering*

2015, *26*, 015002.

(65) Zhang, Y.; Jiang, H.; Zhao, X.; Yan, Y.; Zhang, W.; Li, Y. Characteristics Of The Energetic Micro-Initiator Through Integrating Al/Ni Nano-Multilayers With Cu Film Bridge. *Nanoscale Research Letters* 2017, 12.

(66) Jacob, R.; Jian, G.; Guerieri, P.; Zachariah, M. Energy Release Pathways In Nanothermites Follow Through The Condensed State. *Combustion and Flame* 2015, *162*, 258-264.

(67) Brotman, S.; Rouhani, M.; Rossi, C.; Estève, A. A Condensed Phase Model Of The Initial Al/Cuo Reaction Stage To Interpret Experimental Findings. *Journal of Applied Physics* 2019, *125*, 035102.

(68) Shen, J.; Qiao, Z.; Wang, J.; Yang, G.; Chen, J.; Li, Z.; Liao, X.; Wang, H.; Zachariah, M. Reaction Mechanism Of Al-Cuo Nanothermites With Addition Of Multilayer Graphene. Thermochimica Acta 2018, 666, 60-65.

(69) Deng, S.; Jiang, Y.; Huang, S.; Shi, X.; Zhao, J.; Zheng, X. Tuning The Morphological, Ignition And Combustion Properties Of Micron-Al/Cuo Thermites Through Different Synthesis Approaches. *Combustion and Flame* 2018, 195, 303-310.

(70) Jacob, R.; Ortiz-Montalvo, D.; Overdeep, K.; Weihs, T.; Zachariah, M. Incomplete Reactions In Nanothermite Composites. *Journal of Applied Physics* 2017, *121*, 054307.

(71) Wen, J.; Ringuette, S.; Bohlouli-Zanjani, G.; Hu, A.; Nguyen, N.; Persic, J.; Petre, C.; Zhou, Y. Characterization Of Thermochemical Properties Of Al Nanoparticle And Nio Nanowire Composites. *Nanoscale Research Letters* 2013, 8.

(72) Levitas, V.; Asay, B.; Son, S.; Pantoya, M. Melt Dispersion Mechanism For Fast Reaction Of Nanothermites. *Applied Physics Letters* 2006, *89*, 071909.

(73) Petre, C.; Chamberland, D.; Ringuette, T.; Ringuette, S.; Paradis, S.; Stowe, R. LOW-POWER LASER IGNITION OF ALUMINUM/METAL OXIDE NANOTHERMITES. *International*

Journal of Energetic Materials and Chemical Propulsion 2014, *13*, 479-494.

(74) Zhang, W.; Yin, B.; Shen, R.; Ye, J.; Thomas, J.; Chao, Y. Significantly Enhanced Energy Output From 3D Ordered Macroporous Structured Fe2o3/Al Nanothermite Film. *ACS Applied Materials & Interfaces* 2013, 5, 239-242.

(75) Abdallah, I.; Zapata, J.; Lahiner, G.; Warot-Fonrose, B.; Cure, J.; Chabal, Y.; Esteve, A.; Rossi, C. Structure And Chemical Characterization At The Atomic Level Of Reactions In Al/Cuo Multilayers. *ACS Applied Energy Materials* 2018, 1, 1762-1770.

(76) Wang, Y.; Song, X.; Jiang, W.; Deng, G.; Guo, X.; Liu, H.; Li, F. Mechanism For Thermite Reactions Of Aluminum/Iron-Oxide Nanocomposites Based On Residue Analysis. *Transactions of Nonferrous Metals Society of China* 2014, *24*, 263-270.

(77) Plantier, K.; Pantoya, M.; Gash, A. Combustion Wave Speeds Of Nanocomposite Al/Fe2o3: The Effects Of Fe2o3 Particle Synthesis Technique. *Combustion and Flame* 2005, 140, 299-309.

(78) Egan, G.; Zachariah, M. Commentary On The Heat Transfer Mechanisms Controlling Propagation In Nanothermites. *Combustion and Flame* 2015, 162, 2959-2961.

(79) Trunov, M.; Schoenitz, M.; Dreizin, E. Effect Of Polymorphic Phase Transformations In Alumina Layer On Ignition Of Aluminium Particles. *Combustion Theory and Modelling* 2006, 10, 603-623.

(80) Stamatis, D.; Ermoline, A.; Dreizin, E. A Multi-Step Reaction Model For Ignition Of Fully-Dense Al-Cuo Nanocomposite Powders. *Combustion Theory and Modelling* 2012, 16, 1011-1028.